JOURNAL OF GUIDANCE, CONTROL, AND DYNAMICS
Vol. 40, No. 11, November 2017

Unmanned Aerial Vehicle Guidance for an All-Aspect Approach to a Stationary Point

Satadal Ghosh,* Oleg A. Yakimenko,† and Duane T. Davis‡
Naval Postgraduate School, Monterey, California 93943
and
Timothy H. Chung§
Defense Advanced Research Projects Agency, Arlington, Virginia 22203

DOI: 10.2514/1.G002614

This paper offers an integrated framework enabling planar and spatial guidance for a fixed-wing aerial vehicle to approach a stationary point from any direction. Specifically, it elaborates on the standard and two-stage pure proportional navigation guidance laws developed earlier and proposes an integrated multiphase planar guidance scheme for the all-aspect approach while also accounting for an onboard seeker's field-of-view limitation. This scheme is further extended to a two-plane-segregated two-planar-phase guidance scheme for achieving any terminal approach vector at a stationary point in three-dimensional space. The developed algorithms are evaluated in computer and software-in-the-loop simulations involving a model of a small unmanned aerial vehicle equipped with a commercial-off-the-shelf autopilot.

Nomenclature

a	=	lateral acceleration, m/s^2
$\boldsymbol{a}$	=	lateral acceleration vector, m/s^2
B	=	bias, m/s^2
$\boldsymbol{e}$	=	unit vector
$\boldsymbol{e}_P$	=	unit vector along unmanned aerial vehicle's velocity vector
N	=	navigation gain
N_s	=	switched navigation gain in two-stage pure proportional navigation
R	=	range, m
$\boldsymbol{r}$	=	line-of-sight vector, m
$\boldsymbol{r}_P$	=	unmanned aerial vehicle's position vector, m
$\boldsymbol{r}_T$	=	target's position vector, m
t	=	time, s
t_2, t_3, t_4, t_5	=	initiation times of the second through fifth phases, s
$u(t)$	=	step function
V	=	speed, m/s
$\boldsymbol{v}$	=	velocity vector, m/s
α_P	=	unmanned aerial vehicle's heading angle in the engagement plane, rad
$\alpha_{P_2}, \alpha_{P_3}, \alpha_{P_4}, \alpha_{P_5}$	=	unmanned aerial vehicle's headings at the beginning of the second through fifth phases, rad
θ	=	line-of-sight angle, rad
$\theta_2, \theta_3, \theta_4, \theta_5$	=	line-of-sight angles at the beginning of the second through fifth phases, rad
$\mu \triangleq \alpha_P - \theta$	=	unmanned aerial vehicle's look angle, rad
$\mu_2, \mu_3, \mu_4, \mu_5$	=	unmanned aerial vehicle's look angles at the beginning of the second through fifth phases, rad
μ_s	=	unmanned aerial vehicle's onboard seeker field-of-view constraint, rad
$\boldsymbol{\Omega}$	=	line-of-sight angular rotation vector, rad/s
ω	=	magnitude of angular rotation of line of sight, rad/s

Subscripts

f	=	final value
P	=	unmanned aerial vehicle
$p1, p2$	=	the first and second planar phases in a three-dimensional scenario
$\boldsymbol{r}$	=	along-range vector
T	=	target
$\boldsymbol{t}$	=	along transverse direction to the range vector
$\boldsymbol{\Omega}$	=	along line-of-sight angular rotation vector
0	=	initial value

Superscript

d	=	desired value

I. Introduction

THE terminal path angle has been mostly studied in the literature in the context of interceptor guidance, and it has been termed as the impact angle. It is defined as the angle between the interceptor's velocity vector and a predefined reference at the time of interception of the targets. For stationary targets, this predefined reference may be the inertial reference axis; for moving targets, it usually coincides with the target's velocity direction at the time of interception. Besides ensuring a sufficiently low miss distance, control of the impact angle has become a necessity in modern-day warfare for various reasons like enhancement of warhead effectiveness, directional kill mechanism of interceptors, avoidance of target defense mechanisms and countermeasures, facilitating seeker acquisition, etc.

Similar to the interceptor–target engagement problems, for unmanned aerial vehicles (UAVs), controlling terminal path angles is also important. This necessity could be dictated by various requirements like efficient waypoint navigation, achieving rendezvous, and/or other desired formations following a trajectory with a sensing and/or tracking vantage, etc. Current literature [1–7] on trajectory control of UAVs highlights the utility of guidance laws, which are discussed mostly in the context of interceptor–target engagements for the purpose of motion control of UAVs to follow desired paths. In this context, impact angle-constrained guidance

Received 15 November 2016; revision received 5 April 2017; accepted for publication 7 April 2017; published online 24 July 2017.

*U.S. National Research Council Research Associate, Department of Systems Engineering; sghosh@nps.edu.
†Professor, Department of Systems Engineering; oayakime@nps.edu. Associate Fellow AIAA.
‡Assistant Professor, Cyber Academic Group; dtdavi1@nps.edu.
§Program Manager, Tactical Technology Office, Defense Advanced Research Projects Agency; timothy.chung@darpa.mil.

algorithms could also be leveraged efficiently for controlling the terminal approach (impact) angle of UAVs.

The impact angle-constrained guidance problem has been dealt with in several ways in the literature. Linear quadratic optimal-control and differential game frameworks were explored for terminal angle control in [8–15]. The limitation on an UAV's onboard seeker's field of view (FOV) was considered in an optimal-control-based guidance formulation for impact angle control in [16]. The notion of a zero-effort collision triangle was incorporated in a linear optimal guidance problem in [17]. These analyses considered a linearized version of the nonlinear kinematics of an interceptor–target engagement, whereas the nonlinearity of this problem was dealt with using the state-dependent Riccati equation technique in [18,19] for stationary and maneuvering targets, respectively. Usually, implementation of these optimal-control-based guidance laws is sensitive to the time-to-go estimation error. Several sliding-mode-control-based guidance laws were developed in [20–24] for impact angle control under different engagement considerations. A fuzzy-logic-based formulation [25] was also developed for this purpose. Most of the modern guidance laws have difficulty of implementation because of either the sensitivity with respect to guidance command parameters or the burden of real-time onboard computation. Another class of guidance laws, which rely on line-of-sight (LOS) information, usually provides more appealing algorithms for real-time implementation. Proportional navigation (PN) and its several variations, as well as a few other algorithms, fall within this category. Several PN-based guidance laws, like a time-varying biased pure PN [26], an adaptive PN in two orthogonal planes in a three-dimensional (3-D) engagement [27], a two-stage planar pure PN (2pPPN) for stationary and lower-speed targets [28,29], an integrated form of the biased pure PN [30], a composite PN-based guidance for higher-speed targets [31], and an anticipatory augmented pure PN for maneuvering targets [32], were presented for impact angle control. To deal with the limitation of the interceptor's onboard seeker's FOV, look-angle constraints were embedded in the PN-based impact angle-control guidance formulations in the form of gain and/or bias shaping [33–35]. Other variants of PN to achieve a desired terminal angle, circular navigation [36], and relative circular navigation [37] were also studied. A planar three-point trajectory shaping guidance law [38] based on LOS information against the stationary targets was also developed to achieve a required impact angle.

Most of the literature on impact angle-constrained guidance has dealt with scenarios against the stationary targets, like aircraft carrier warships that are armored heavily and equipped with efficient electronic countermeasures and close-in weapons systems. Hence, besides other demanding capabilities, controlling the impact angle also becomes essential to achieve successful interception against such stationary or comparatively slowly moving targets. This necessity, apart from mathematical tractability, justifies more focus of a large part of the existing literature on the impact angle control against the stationary targets. However, these studies were mainly motivated by interceptor–target engagements, in which the angles between the initial LOS and UAV's velocities V_{P_0} and V_{P_f} had a different sign (see Fig. 1). As a result, these studies led to the guidance laws with achievable impact angles within a semicircle $[-\pi+\theta_0, \theta_0)$, denoted as regions I and II in Fig. 1 (angular intervals $[2\theta_0-\alpha_{P_0}, \theta_0)$ and $[-\pi+\theta_0, 2\theta_0-\alpha_{P_0})$, respectively), but not the entire angular spectrum $[-\pi, \pi)$ (where θ_0 is the initial LOS angle), which might be required for an UAV approaching some arbitrary point in space. The only few exceptions were [9,10,14,16], which used optimal-control-based guidance; [21,23], and [24] that used sliding-mode-control-based guidance; [36,37] which employed circular navigation; and [39–41] that leveraged the Dubins curve-based approach. The optimal-control-based approaches rely on linearization of nonlinear engagement problem and are sensitive to the time-to-go estimation error, while the sliding-mode-based approaches have limitations in dealing with scenarios with a relatively large initial heading error causing a positive initial range rate; and for circular navigation, the maneuver loads become too high at the end of the engagement. Besides these, most of these studies (except [24,41]) considered the impact angle-control problem for two-dimensional (2-D) engagements, and only [16] considered the FOV constraints.

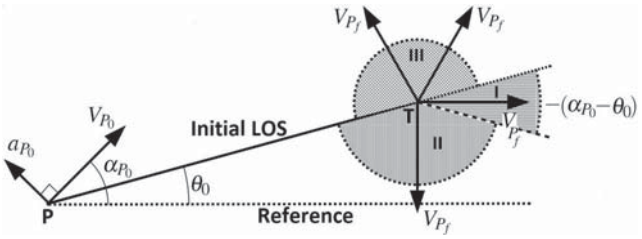

Fig. 1 2-D engagement geometry and UAV's terminal heading.

Unlike most of the existing literature, the goal of this paper is to develop an integrated guidance strategy for an UAV in the nonlinear engagement framework that would allow the approach to a stationary target from any direction (that is covering all regions in Fig. 1), starting from any initial relative attitude in both 2-D and 3-D engagements while also accounting for the FOV limitation of the UAV's onboard seeker. Rather than using the impact angle and terminal angle terms, this paper will use a more generic "approach angle" term to emphasize that the stationary target is not necessarily a stationary vehicle but any point in space, so that other terms will make little sense. To achieve the goal, this paper uses several modifications of the PN-based guidance laws that have widely been studied due to their simplicity, efficiency, optimality, inherent robustness, and ease of implementation [42,43], which render the feasibility and operational advantage of the proposed integrated guidance scheme. The paper shows how any-approach-angle guidance would work in the 2-D and 3-D engagements without and with real-world constraints imposed by a UAV's seeker. Specifically, Sec. II of this paper proceeds with reviewing and reintroducing the earlier developed approach angle control that uses planar pure PN (PPN) and two-stage PPN (2pPPN) strategies in the context of any-approach angle engagements. Then, in order to expand the set of achievable approach angles to the full circle of the angular spectrum, reversal of the LOS rotation is found to be crucial, which necessitates a three-phase composite guidance scheme in which the PPN guidance command is enhanced by a suitable bias. Switching from a phase to its subsequent phase is governed by well-defined and straightforward conditions on the LOS turn rate, LOS angle, and desired approach angle, which are established analytically. Moreover, changes in the phases in such engagements provide an additional advantage of flexibility in trajectory shaping. This three-phase composite scheme, combined with PPN and 2pPPN, leads to an integrated, any-approach angle guidance, referred to as approach angle-constrained integrated guidance, or αCIG. Note that the phrase "integrated guidance" is used here to imply the integration of three different guidance strategies: PPN, 2pPPN, and the three-phase composite guidance presented in this paper. Under the limitation of the FOV of the onboard seeker, this composite guidance for an approach angle control is then extended to a look-angle-constrained engagement scenario in Sec. III. Combined with PPN and look-angle-constrained 2pPPN, this results in look-angle-constrained and any-approach angle integrated guidance, referred to as $\mu\alpha$CIG. Next, the developed all-approach angle guidance strategies are reformulated for the 3-D engagement geometry in Sec. IV. In particular, the $\mu\alpha$CIG strategy for planar engagement is extended to a 3-D engagement framework, resulting in a two-plane-segregated two-planar-phase integrated guidance scheme (referred to as $\mu\alpha$CIG3D). Section V presents examples of computer simulations for approach angle/approach vector control in 2-D/3-D engagements, respectively. Finally, the results of a flight-ready software-in-the-loop (SITL) simulation conducted for a small UAV model are presented in Sec. VI.

II. All-Aspect Approach in 2-D

This section considers the basic problem of approach angle control over the entire angular spectrum $[-\pi, \pi)$. The existing literature on approach angle control using PPN and 2pPPN [28], which is required for subsequent analysis, is revisited in Sec. II.B. Then, to expand the

set of achievable approach angles to another half of the angular spectrum, a bias-based augmentation of PPN and 2pPPN leading to a three-phase composite guidance scheme (the main contribution of this section) is presented in Sec. II.C. This scheme is then combined with PPN and 2pPPN, yielding an integrated all-approach angle guidance (αCIG) in Sec. II.D.

A. 2-D Engagement Geometry

Consider the planar engagement geometry depicted in Fig. 1. The UAV P is modeled as a point mass moving with constant speed V_P and approaching a stationary target T. The kinematic equations of motion are expressed in terms of the range R and LOS angle θ between P and T as

$$V_R = \dot{R} = -V_P \cos(\alpha_P - \theta) \tag{1}$$

$$V_\theta = R\dot{\theta} = -V_P \sin(\alpha_P - \theta) \tag{2}$$

$$\dot{\alpha}_P = a_P / V_P \tag{3}$$

where α_P and a_P are the UAV's velocity heading angle and lateral acceleration, respectively. Also, the UAV's look angle, to be used later in this paper, is defined as

$$\mu \triangleq \alpha_P - \theta \tag{4}$$

The UAV's lateral acceleration a_P is based on the pure PN (PPN) guidance law with the navigation gain N given by

$$a_P = V_P \dot{\alpha}_P = N V_P \dot{\theta} \tag{5}$$

The problem under consideration in this section is to develop an integrated guidance strategy for the UAV based on PPN to achieve any approach angle at the stationary target $\alpha_{P_f} \in [-\pi, \pi)$.

B. Review of PPN and 2pPPN Strategies

Without loss of generality, consider the case when $\alpha_{P_0} \geq \theta_0$; that is, $\alpha_{P_0} \in [\theta_0, \theta_0 + \pi)$. First, consider $\alpha_{P_0} \in (\theta_0, \theta_0 + \pi)$. In this case, from Eqs. (3) and (5), it follows that the achievable approach angle using the standard PPN guidance is given by

$$\alpha_{P_f} = \alpha_{P_0} + N(\theta_f - \theta_0) \tag{6}$$

A collision course with a stationary target assumes $\alpha_{P_f} = \theta_f$ [44]. From Eq. (6), it follows that

$$\alpha_{P_f} = (N\theta_0 - \alpha_{P_0})/(N-1) \tag{7}$$

For $N \geq 2$ (which is a condition for bounded terminal lateral acceleration of the UAV [43]), the achievable approach angle using PPN resides in the interval

$$\alpha_{P_f} \in [2\theta_0 - \alpha_{P_0}, \theta_0); \qquad N \geq 2 \tag{8}$$

where α_{P_f} equals $2\theta_0 - \alpha_{P_0}$ when $N = 2$, and it approaches θ_0 when $N \to \infty$. However, it could readily be observed that $[2\theta_0 - \alpha_{P_0}, \theta_0) \subset [-\pi + \theta_0, \theta_0)$, which implies that using the standard PPN, a significant portion of the angular interval in the half-space $[-\pi + \theta_0, \theta_0)$ cannot be achieved, which can be noted from Fig. 1. To expand the achievable approach angle set, a two-stage PPN guidance strategy (2pPPN) was introduced [28]. A result on achievable approach angles and required navigation gains for PPN and 2pPPN is formulated in the following theorem:

Theorem 1: Consider $\alpha_{P_0} > \theta_0$. A desired approach angle $\alpha^d_{P_f} \in [2\theta_0 - \alpha_{P_0}, \theta_0)$ could be attained by PPN with $N = (\alpha^d_{P_f} - \alpha_P)/(\alpha^d_{P_f} - \theta) \geq 2$, whereas $\alpha^d_{P_f} \in [-\pi + \theta_0, 2\theta_0 - \alpha_{P_0})$ could be achieved by 2pPPN with

$$N = \begin{cases} (2/\pi)(\alpha_{P_0} - \theta_0); & \text{if } (\alpha^d_{P_f} - \alpha_P)/(\alpha^d_{P_f} - \theta) < 2 \\ (\alpha^d_{P_f} - \alpha_P)/(\alpha^d_{P_f} - \theta); & \text{if } (\alpha^d_{P_f} - \alpha_P)/(\alpha^d_{P_f} - \theta) \geq 2 \end{cases} \tag{9}$$

Proof: The achievable approach angle set using PPN for $N \geq 2$ is evident from Eq. (8). From Eqs. (6–8), it follows that $(\alpha^d_{P_f} - \alpha_{P_0})/(\alpha^d_{P_f} - \theta_0) < 2$ for $\alpha^d_{P_f} \in [-\pi + \theta_0, 2\theta_0 - \alpha_{P_0})$. In these cases, a suitable guidance is needed in the first stage, which leads to an engagement condition in α_P and θ such that $(\alpha^d_{P_f} - \alpha_P)/(\alpha^d_{P_f} - \theta) \geq 2$ at the end of the first stage. Using $N = (2/\pi)(\alpha_{P_0} - \theta_0)$ during the first stage achieves this purpose; thus, at the second/final stage, PPN with $N = (\alpha^d_{P_f} - \alpha_P)/(\alpha^d_{P_f} - \theta)$ achieves $\alpha^d_{P_f} \in [-\pi + \theta_0, 2\theta_0 - \alpha_{P_0})$. For details of the proof, see [28]. □

Examples of trajectories using PPN for $\alpha^d_{P_f} = -\pi/6$ and 2pPPN for $\alpha^d_{P_f} = -5\pi/6$ are presented in Fig. 2a, with and without the look-angle constraint. Note that, for practical implementation, the initial separation of the UAV and stationary target should be sufficiently high, which is governed by the maximum turn rate of the UAV, the initial LOS rate, the desired terminal angle, and the UAV's speed. Theorem 1 serves as a building block for the multiphase composite guidance strategy developed in the subsequent section. Following a similar methodology for $\alpha_{P_0} \in (-\pi + \theta_0, \theta_0)$, Theorem 1 can be restated as the following observation:

Observation 1: Consider $\alpha_{P_0} < \theta_0$. A desired approach angle $\alpha^d_{P_f} \in (\theta_0, 2\theta_0 - \alpha_{P_0}]$ could be attained by PPN with $N = (\alpha^d_{P_f} - \alpha_P)/(\alpha^d_{P_f} - \theta) \geq 2$, whereas $\alpha^d_{P_f} \in (2\theta_0 - \alpha_{P_0}, \pi + \theta_0]$ could be achieved by 2pPPN with

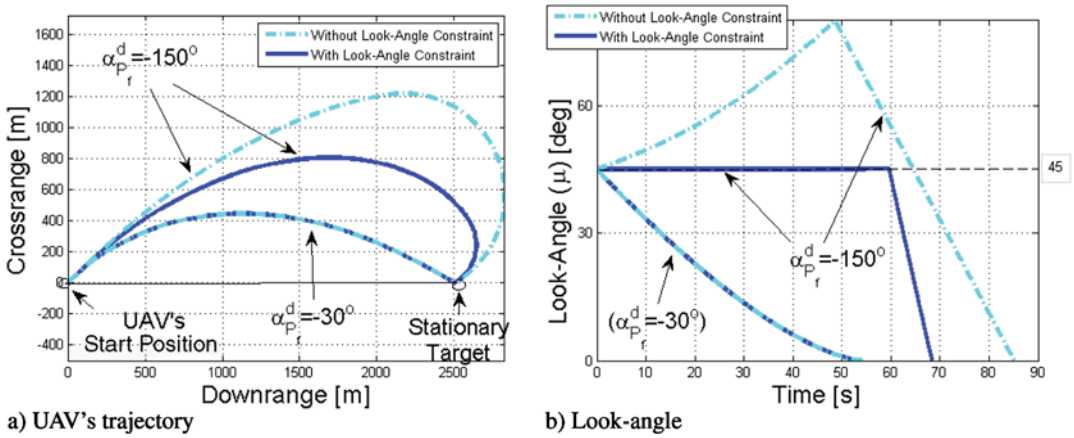

a) UAV's trajectory b) Look-angle

Fig. 2 Examples of PPN and 2pPPN.

$$N = \begin{cases} (2/\pi)|\alpha_{P_0} - \theta_0|; & \text{if } (\alpha^d_{P_f} - \alpha_P)/(\alpha^d_{P_f} - \theta) < 2 \\ (\alpha^d_{P_f} - \alpha_P)/(\alpha^d_{P_f} - \theta); & \text{if } (\alpha^d_{P_f} - \alpha_P)/(\alpha^d_{P_f} - \theta) \geq 2 \end{cases} \tag{10}$$

Now, consider that the initial engagement geometry is already in collision or an inverse collision course, which has not been discussed so far in Theorem 1 and Observation 1. These scenarios imply $\alpha_{P_0} = \theta_0$ or $\alpha_{P_0} = -\pi + \theta_0$, respectively, as follows from Eq. (2). Thus, $\dot{\theta}_0 = 0$; therefore, the PN guidance command is zero. Hence, controlling approach angle from these two initial conditions by using just the LOS turn-rate-based guidance scheme is not possible. To get rid of such a deadlock situation, an engagement geometry outside the collision course needs to be achieved to employ the approach angle-constrained guidance schemes presented in this paper. To achieve this, a finite bias with a suitable sign, termed the "adjustment bias," needs to be applied as described in the next observation.

Observation 2: If $\alpha_{P_0} = \theta_0$ or $\alpha_{P_0} = -\pi + \theta_0$, then before applying Theorem 1 and Observation 1, an engagement geometry (α_P, θ) needs to be attained outside the collision course or inverse collision course such that $\text{sgn}(\alpha_P - \theta) = -\text{sgn}(\alpha^d_{P_f} - \theta)$. This can be accomplished by using a finite adjustment pulse bias B_{adj} satisfying

$$\text{sgn}(B_{\text{adj}}) = \begin{cases} -\text{sgn}(\alpha^d_{P_f} - \theta_0); & \text{if } \alpha_{P_0} = \theta_0 \\ \text{sgn}(\alpha^d_{P_f} - \theta_0); & \text{if } \alpha_{P_0} = -\pi + \theta_0 \end{cases} \tag{11}$$

C. Three-Phase Composite Guidance

To expand the set of achievable approach angles to another half of the angular spectrum beyond the achievable approach angle set using PPN and 2pPPN, the reversal of the LOS rotation is found to be crucial in this section. It is shown to be successfully attained by addition of a suitable bias to the PPN guidance command during the first phase of engagement. This leads to a three-phase composite guidance scheme. This section provides these major results that will help in formulating the integrated all-approach-angle guidance law in Sec. II.D.

Lemma 1: For the PPN guidance command [Eq. (5)] against a stationary target, $\dot{\theta}$ keeps the same sign during the entire engagement.

Proof: From Eqs. (2–4), $\dot{\mu}$ is given by

$$\dot{\mu} = -(N-1)V_P \sin\mu/R \tag{12}$$

Clearly, from Eq. (12), if $N > 1, \dot{\mu} < 0$ for $\mu \in (0, \pi)$, and $\dot{\mu} > 0$ for $\mu \in (-\pi, 0)$. From Eqs. (1) and (12), the differential evolution of range R with respect to μ is given as

$$\begin{aligned} \text{d}R/\text{d}\mu &= R\cot\mu/(N-1) \\ \Rightarrow R &= (R_0/|\sin\mu_0|^{(1/(N-1))})|\sin\mu|^{(1/(N-1))} \end{aligned} \tag{13}$$

Hence, for $N > 1, R = 0$ is equivalent to $\mu = 0$. Relations (12) and (13) imply that μ monotonically decreases to zero at intercept if $\mu_0 \in (0, \pi)$, and it monotonically increases to zero at intercept if $\mu_0 \in (-\pi, 0)$. Because μ belonging to $(-\pi, 0)$ or $(0, \pi)$ means $\dot{\theta} > 0$ or $\dot{\theta} < 0$, respectively, from Eq. (2), θ remains sign-preserving throughout the entire engagement.

From Eq. (12), it can also be noted that, for $N < 1$, μ varies monotonically but still remains within the same half-space $(-\pi, 0)$ or $(0, \pi)$. Therefore, from Eq. (2), $\dot{\theta}$ keeps the same sign. Also, for $N = 1, \mu$ remains constant, following Eq. (12); hence, from Eq. (2), $\dot{\theta}$ remains sign-preserving. □

Lemma 1 shows that, for standard PPN or 2pPPN, the LOS rate does not change its sign. However, to achieve $\alpha^d_{P_f}$ in the same half-space as α_{P_0}, shown as region III in Fig. 1 (that is, to achieve $\alpha^d_{P_f} \in [\theta_0, \pi + \theta_0)$ or $\alpha^d_{P_f} \in (-\pi + \theta_0, \theta_0]$ when α_{P_0} also belongs to $[\theta_0, \pi + \theta_0)$ or $(-\pi + \theta_0, \theta_0]$, respectively), the trajectories necessitate a change in the sign of the LOS rate (see Case 3 in Fig. 3a). Now, the existence of a PN-based guidance command would be discussed, which helps in the conversion of the sign of the LOS rate at some time instant before terminal approach to the stationary target.

Lemma 2: Addition of a finite bias profile $B\text{sgn}(\dot{\theta}_0)$, with B finite and positive for a certain time interval, to the PPN guidance command [Eq. (5)] with $N > 2$ results in reversing the sign of $\dot{\theta}$.

Proof: From Eq. (2) and Lemma 1, it is evident that there exists a time t_1 during the engagement from which time $|\sin\mu|$, and hence $|\dot{\theta}|$, monotonically decreases and becomes zero at the end. Note that, for $\mu_0 > \pi/2$ (or $\mu_0 < -\pi/2$), this time t_1 signifies $\mu(t_1) = \pi/2$ (or $\mu(t_1) = -\pi/2$); otherwise, $t_1 = t_0$. Now, consider the guidance command of the UAV as

$$a_P = NV_P\dot{\theta} + B\text{sgn}(\dot{\theta}_0)u(t - t_1) \tag{14}$$

where B is a positive finite bias. From Eq. (2), $\mu_0 > 0$ ($\mu_0 < 0$) implies that $\dot{\theta}_0 < 0$ ($\theta_0 > 0$). Therefore, from Eqs. (12) and (14),

$$\begin{aligned} &\dot{\mu} = -(N-1)V_P \sin\mu/R + (B/V_P)\text{sgn}\dot{\theta}_0 \Rightarrow \\ &\frac{\text{d}|\mu|}{\text{d}t} < -(N-1)V_P|\sin\mu|/R \end{aligned} \tag{15}$$

From Eqs. (12) and (15), $|\mu|$ decreases at a higher rate as compared to that of the standard PPN. Recall from Lemma 1 that, for standard PPN against a stationary target, both $|\mu|$ and R go to zero simultaneously. However, using the bias as in Eq. (14), $|\mu|$ reaches zero faster than R and crosses a zero value due to nonzero positive B in a_P that, following Eq. (2), implies that $\dot{\theta}$ changes sign before R goes to zero. □

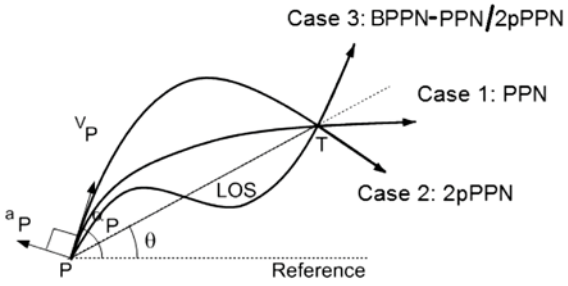

a) Possible terminal heading of UAV at stationary target

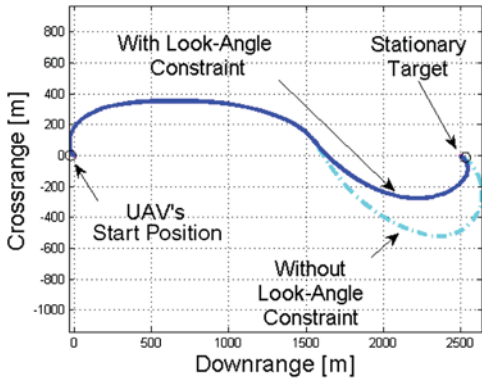

b) UAV's trajectory for $\alpha^d_{P_f} = 5\pi/6$

Fig. 3 Possible terminal approach geometry and an example of three-phase composite guidance.

Thus, Lemma 2 helps formulating the biased PPN (BPPN) guidance law for the initial phase of engagement to ensure a change of the sign of the LOS rate (before final approach to a stationary target) at time t_2 with LOS angle θ_2 and the UAV's heading angle $\alpha_{P_2}(=\theta_2)$ at which the LOS rate changes its sign.

Consider $\alpha^d_{P_f} \in [\theta_0, \pi+\theta_0)$ and $\alpha_{P_0} > \theta_0$. Then, $\dot{\theta}$ is negative in the first phase of the engagement, which implies that $\theta_2 < \theta_0$, and so is α_{P_2}. However, for time t_2 onward, $\dot{\theta}$ becomes positive, and hence θ starts increasing from the value θ_2. If α_P keeps on decreasing during this time, μ remains negative, and hence $\dot{\theta}$ remains positive [see Eq. (2)]. Following Observation 1, during this time, for any θ, $\alpha_{P_f} \in (\theta, \pi+\theta]$. Then, the union of all such intervals for θ varying from θ_2 to θ_0 is given by

$$\cup_{\theta=\theta_2<\theta_0}^{\theta_0} (\theta, \pi+\theta] = (\theta_2, \pi+\theta_0] \supset [\theta_0, \pi+\theta_0) \tag{16}$$

Now, consider an angle θ_3 from the set $\{\theta \in (\theta_2, \theta_0] \,|\alpha^d_{P_f} \in [\theta_0, \pi+\theta)\}$. If the final phase begins with θ_3 and α_{P_3} such that $\alpha_{P_3} < \theta_3$, then following Observation 1, the desired approach angle is achievable by using the standard PPN or 2pPPN as suitable in the final phase. A similar logic also follows in the intermediate phase for $\alpha_{P_0} < \theta_0$. The preceding discussion leads to the BPPN guidance command for the UAV during the second phase formulated in the following observation, such that it is ensured that α_P monotonically varies during this intermediate phase.

Observation 3: Consider $\alpha_{P_0} > \theta_0$ ($\alpha_{P_0} < \theta_0$). A guidance command $a_P = NV_P\dot{\theta} + B\text{sgn}(\theta_0)u(t-t_2)$, where $B > 0$ at $t = t_2$, implies $\dot{\mu}_2 < 0$ ($\dot{\mu}_2 > 0$), and $N < 1, B > 0$, for $t > t_2$ lead to either an increase (decrease) in α_P at a slower rate than θ or a decrease (increase) in α_P following Eq. (3). This results in a decrease (increase) in μ, and hence increase (decrease) in θ, during the second phase.

The following theorem combines BPPN in first two phases followed by PPN or 2pPPN as suitable in the final phase to yield a three-phase composite guidance strategy to achieve the other half-space of approach angles $[\theta_0, \pi+\theta_0)$.

Theorem 2: Let $\alpha_{P_0} > \theta_0$. Using BPPN guidance laws, as given in Lemma 2 and Observation 3, for the first two phases, respectively, followed by the standard PPN or 2pPPN, as mentioned in Observation 1, any approach angle belonging to the set $[\theta_0, \pi+\theta_0)$ can be achieved.

Proof: Following Lemma 2 and Observation 3, using $a_P = NV_P\dot{\theta} + B\text{sgn}(\dot{\theta}_0)$ with $N = 2$ in the first phase and $N < 1$ in the second phase, as well as $B > 0$ in both the first and second phases, an engagement condition $(\alpha_P, \theta) = (\alpha_{P_3}, \theta_3)$ is obtained at the end of the second phase (say, at time t_3) such that $\theta_2 < \theta_3 \le \theta_0$, $\alpha_{P_3} < \theta_3$, and

$$\alpha^d_{P_f} \in (\theta_3, \pi+\theta_3] \cap [\theta_0, \pi+\theta_0) = [\theta_0, \pi+\theta_3]$$

Therefore, following Observation 1, $\alpha^d_{P_f} \in [\theta_0, 2\theta_3 - \alpha_{P_3}]$ can be achieved using standard PPN with $N = (\alpha^d_{P_f} - \alpha_{P_3})/(\alpha^d_{P_f} - \theta_3) \ge 2$, whereas $\alpha^d_{P_f} \in (2\theta_3 - \alpha_{P_3}, \pi+\theta_3)$ could be achieved using 2pPPN with $N = (2/\pi)|\alpha_{P_3} - \theta_3|$ if $(\alpha^d_{P_f} - \alpha_P)/(\alpha^d_{P_f} - \theta) < 2$, and it is equal to $(\alpha^d_{P_f} - \alpha_P)/(\alpha^d_{P_f} - \theta)$ otherwise. □

An example of the trajectory generated by the three-phase composite guidance strategy of Theorem 2 is shown in Fig. 3b for $\alpha^d_{P_f} = 5\pi/6 \in [\theta_0, \pi+\theta_0) = [0, \pi)$ without any look-angle constraint.

Observation 4: Following a similar argument as given previously for $\alpha_{P_0} > \theta_0$, it can also be shown that, using BPPN guidance laws for $\alpha_{P_0} < \theta_0$, as given in Lemma 2 and Observation 3, for the first two phases, respectively, followed by the standard PPN or 2pPPN, as mentioned in Theorem 1, any approach angle belonging to the set $(-\pi+\theta_0, \theta_0]$ can be achieved.

Observation 5: From Observation 3 and its preceding discussion, it can be noted that, for $\alpha_{P_0} > \theta_0$ ($\alpha_{P_0} < \theta_0$), if α_P decreases (increases) in the second phase, μ remains negative (positive) until α_P decreases (increases) to $-\pi+\theta$ ($\pi+\theta$) for some $\theta = \bar{\theta}_3 \in (-\pi+\theta_0, \theta_0)$ ($\bar{\theta}_3 \in (\theta_0, \pi+\theta_0)$). Therefore, θ_3 may actually be selected from the $(\theta_2, \bar{\theta}_3)$ interval [$(\bar{\theta}_3, \theta_2)$ interval], which would ensure achieving $\alpha^d_{P_f} \in [\theta_0, \pi+\theta_0)$ ($\alpha^d_{P_f} \in (-\pi+\theta_0, \theta_0]$) following Theorem 2 (Observation 4). However, selection of θ_3 closer to $\bar{\theta}_3$ might lead to an unnecessary delay in the final approach and an increase in the overall control energy requirement. Therefore, a selection of θ_3 in some neighborhood of θ_0 could be considered as a judicious option.

Observation 5 yields a justified criteria for the removal of bias in the second phase.

D. αCIG Law and Algorithm

Based on the results presented in Secs. II.B and II.C, the overall guidance strategy (αCIG) can now be presented by the following theorem.

Theorem 3: Using PPN or 2pPPN as mentioned in Theorem 1 and Observation 1 or the three-phase composite guidance strategy given in Theorem 2 and Observation 4, for $\alpha_{P_0} > \theta_0$ and $\alpha_{P_0} < \theta_0$, respectively, an expanded approach angle set $[-\pi, \pi)$ can be achieved.

Proof: The proof follows from Theorems 1 and 2 for $\alpha_{P_0} > \theta_0$ and Observations 1 and 4 for $\alpha_{P_0} < \theta_0$. □

Considering Theorems 1–3 and Observations 1–5, the αCIG algorithm for initial engagement geometries different than the collision or inverse collision course can now be formulated as follows.

Given α_{P_0} and $\alpha^d_{P_f}$,

1) Use the standard PPN $a_P^{\alpha CIG} = NV_P\dot{\theta}$ with $N = (\alpha^d_{P_f} - \alpha_{P_0})/(\alpha^d_{P_f} - \theta_0)$ if $\alpha^d_{P_f} \in [2\theta_0 - \alpha_{P_0}, \theta_0)$ or $\alpha^d_{P_f} \in (\theta_0, 2\theta_0 - \alpha_{P_0}]$ for $\alpha_{P_0} > \theta_0$ or $\alpha_{P_0} < \theta_0$, respectively.

2) Use 2pPPN $a_P^{\alpha CIG} = NV_P\dot{\theta}$ with $N = (2/\pi)|\alpha_{P_0} - \theta_0|$ as long as $(\alpha^d_{P_f} - \alpha_P)/(\alpha^d_{P_f} - \theta) < 2$ and use $N = (\alpha^d_{P_f} - \alpha_P)/(\alpha^d_{P_f} - \theta)$ otherwise, if $\alpha^d_{P_f} \in [-\pi+\theta_0, 2\theta_0 - \alpha_{P_0})$ or $\alpha^d_{P_f} \in (2\theta_0 - \alpha_{P_0}, \pi+\theta_0]$ for $\alpha_{P_0} > \theta_0$ or $\alpha_{P_0} < \theta_0$, respectively.

3) Else, use the following proposed three-phase composite guidance scheme:

a) In the first phase, use the BPPN guidance $a_P^{\alpha CIG} = NV_P\dot{\theta} + B\text{sgn}(\dot{\theta}_0)$ with $N = 2$ and bias $B > 0$ until $\dot{\theta}$ changes sign; let, at $t = t_2$, $\theta = \theta_2$, and $\alpha_P = \alpha_{P_2}$. Start the second phase as in Step 3b.

b) Select $\theta_3 \in (\theta_2, \theta_0]$ or $\theta_3 \in [\theta_0, \theta_2)$ such that $\alpha^d_{P_f} \in [\theta_0, \theta_3 + \pi]$ or $\alpha^d_{P_f} \in [-\pi+\theta_3, \theta_0]$ for $\alpha_{P_0} > \theta_0$ or $\alpha_{P_0} < \theta_0$, respectively. In the second phase, use the BPPN guidance $a_P^{\alpha CIG} = NV_P\dot{\theta} + B\text{sgn}(\dot{\theta}_0)$ with $N < 1$ and bias $B > 0$ until θ becomes equal to θ_3; let, at time t_3, when $\alpha_P = \alpha_{P_3}$. Start the third phase as in Step 3c.

c) Use standard PPN $a_P^{\alpha CIG} = NV_P\dot{\theta}$ with $N = (\alpha^d_{P_f} - \alpha_{P_3})/(\alpha^d_{P_f} - \theta_3)$ in the third phase if $\alpha^d_{P_f} \in [\theta_0, 2\theta_3 - \alpha_{P_3}]$ or $\alpha^d_{P_f} \in [2\theta_3 - \alpha_{P_3}, \theta_0]$ for $\alpha_{P_0} > \theta_0$ or $\alpha_{P_0} < \theta_0$, respectively. Otherwise, go to Step 3d.

d) Use 2pPPN $a_P^{\alpha CIG} = NV_P\dot{\theta}$ with navigation gain $N = (2/\pi)|\alpha_{P_3} - \theta_3|$ as long as $(\alpha^d_{P_f} - \alpha_P)/(\alpha^d_{P_f} - \theta) < 2$ and $N = (\alpha^d_{P_f} - \alpha_P)/(\alpha^d_{P_f} - \theta)$ otherwise, if $\alpha^d_{P_f} \in (2\theta_3 - \alpha_{P_3}, \pi+\theta_3)$ or $\alpha^d_{P_f} \in (-\pi+\theta_3, 2\theta_3 - \alpha_{P_3})$ for $\alpha_{P_0} > \theta_0$ or $\alpha_{P_0} < \theta_0$, respectively.

III. All-Aspect FOV-Constrained Approach in 2-D

Even though the initial heading error of the UAV is pretty high, and the target location information is fed from other sources like ground-based radar or telemetry systems, it is desired for autonomous aerial missions with UAVs that, after some time during engagement, the vehicle is oriented in such a way that the target is acquired by its own seeker. Visual servoing is one such situation in which the onboard camera is used as a seeker for visually sensing the target and then computing the required parameters to generate the control command input. However, such seekers have their limitation in terms of their FOVs. Now that the αCIG algorithm has been developed, the real-world limitation imposed by the aerial vehicle's seeker needs to be accounted for. This limitation can be modeled by constraining the look angle (representing the angle between the LOS and the UAV's velocity vectors [Eq. (4)]) so that $\mu \in (-\mu_s, \mu_s)$. To this end, first, the results on the FOV-constrained approach angle control using PPN

and a two-stage PPN (2pPPN) are revisited briefly in Sec. III.A. Then, the major result on the existence of a bias function with state-dependent bounds to achieve a look-angle-constrained approach angle control leading to FOV-constrained bias-shaped three-phase composite guidance is presented in Sec. III.B. A computationally inexpensive, and hence easily real-time implementable, methodology for bias shaping from the set of feasible bias profiles is also suggested. Finally, this composite guidance scheme is combined with PPN and 2pPPN, yielding an integrated FOV-constrained all-approach angle guidance ($\mu\alpha$CIG) in Sec. III.C.

A. Preliminary Observations

Without loss of generality, consider $\mu_0 > 0$. Note from Eq. (12) that, for $N > 1$, μ monotonically decreases with time for $\mu \in (0, \pi)$, which implies that, once the stationary target is within the UAV's FOV, it will always remain within it. Therefore, keeping in mind the bounded final lateral acceleration of the UAV with $N \geq 2$, it is ensured that the UAV's seeker is able to lock onto the target at some time point during engagement. For $\mu_0 \in (0, \mu_s)$, the UAV with $N \geq 2$ successfully approaches the stationary target with $\alpha_{P_f} \in [2\theta_0 - \alpha_{P_0}, \theta_0)$, as shown in Eq. (8).

On the other hand, for $N = 1$, according to Eq. (12), μ remains constant. With this observation and the fact that PPN with $N = 1$ leads to an engagement condition with the LOS angle θ anywhere in the interval $[-\pi, 0)$, a two-stage PPN-based guidance strategy, referred to as look-angle-constrained 2pPPN, was devised in [35] to expand the set of achievable approach angles to $[-\pi + \theta_0, \theta_0)$ while maintaining the FOV constraint. Considering that the UAV's seeker has already locked onto the target, which could be guaranteed by choosing $N > 1$, as discussed previously, the following theorem can be formulated.

Theorem 4: Consider $\mu_0 = \alpha_{P_0} - \theta_0 \in (0, \mu_s)$. Any $\alpha^d_{P_f} \in [2\theta_0 - \alpha_{P_0}, \theta_0)$ could be attained in a look-angle-constrained manner using PPN with $N \geq 2$. And, any $\alpha^d_{P_f} \in [-\pi + \theta_0, 2\theta_0 - \alpha_{P_0})$ could be achieved while maintaining the FOV constraint by applying the look-angle-constrained 2pPPN with

$$N = \begin{cases} 1; & \text{if } \theta \in (\alpha^d_{P_f} + \mu_0/(N_s - 1), \theta_0]; \quad \text{for some switched gain } N_s \geq 2 \\ N_s; & \text{otherwise} \end{cases} \tag{17}$$

where $N_s \geq 2$ represents the switched navigation gain at the second stage of 2pPPN.

Proof: For details of the proof, see [35]. □

Examples of look-angle-constrained trajectories that use PPN and 2pPPN are presented in Fig. 2a for $\alpha^d_{P_f} = -\pi/6, -5\pi/6$, respectively, where $\mu_s = \pi/4$. Note that the 2pPPN trajectory for $\alpha^d_{P_f} = -5\pi/6$ changes if the look-angle constraint is applied, whereas the PPN trajectory for $\alpha^d_{P_f} = -\pi/6$ remains the same. The variation of look angles over time is given in Fig. 2b. Following a similar approach as in Theorem 4, the achievable approach angles and navigation gain values with initial conditions $\mu_0 < 0$ can be restated as in the following observation.

Observation 6: Consider $\mu_0 \in (-\mu_s, 0)$. Any $\alpha^d_{P_f} \in (\theta_0, 2\theta_0 - \alpha_{P_0}]$ could be attained using PPN with $N = (\alpha^d_{P_f} - \alpha_P)/(\alpha^d_{P_f} - \theta) \geq 2$ while satisfying the FOV constraint. On the other hand, $\alpha^d_{P_f} \in (2\theta_0 - \alpha_{P_0}, \pi + \theta_0]$ could be achieved using look-angle-constrained 2pPPN with

$$N = \begin{cases} 1; & \text{if } \theta \in [\theta_0, \alpha^d_{P_f} + \mu_0/(N_s - 1)); \quad \text{for some } N_s \geq 2 \\ N_s; & \text{otherwise} \end{cases} \tag{18}$$

For the initial conditions $\mu_0 = 0$ or $\mu_0 = \pm\pi$, a finite adjustment pulse bias B_{adj}, similar to that described in Observation 2, needs to be applied at the beginning of engagement to obtain an engagement geometry (α_P, θ) outside the collision or inverse collision course and satisfying $|\mu| = |\alpha_P - \theta| < \mu_s$.

B. FOV-Constrained Bias-Shaped Three-Phase Composite Guidance

Consider $\mu_0 > 0$, and thus $\dot{\theta}_0 < 0$. Then, for $N \geq 2$ and $B > 0$, μ decreases monotonically to zero following Eq. (15). This implies that the conditions in Lemma 2 ensure that, once the target comes within the FOV of the UAV, it remains in there throughout the first phase, which ends at time t_2 when μ just crosses zero ($\dot{\theta}$ just changes its sign). Then, the purpose of the second phase is to ensure the decrease of μ such that $-\mu_s < \mu < 0$ throughout the second phase and an engagement condition (α_{P_3}, θ_3) at the end of the second phase satisfying $\alpha^d_{P_f} \in [\theta_0, \pi + \theta_3]$ and $\mu_3 = \alpha_{P_3} - \theta_3 \in (-\mu_s, 0)$ so that using PPN or look-angle-constrained 2pPPN during the third phase is sufficient to achieve the desired approach angle with the look-angle constraint. To this end, the following major results prove the existence of a bias-shaped BPPN in the second phase leading to the FOV-constrained bias-shaped composite guidance scheme.

Lemma 3: Consider $\mu_0 \in (0, \mu_s)$. There exists a guidance command to the UAV in the second phase $a_P = NV_P\dot{\theta} + B\text{sgn}(\dot{\theta}_0)u(t - t_2)$, where $N < 1$ and bias profile B is a function of time with state-dependent bounds until some time $t_3 > t_2$, with $B > 0$ at time $t = t_2$, such that θ monotonically increases to some value $\theta_3 \triangleq \theta(t_3)$ that satisfies $\alpha^d_{P_f} \in [\theta_0, \pi + \theta_3)$, and μ monotonically decreases to a value $\mu_3 \triangleq \alpha_P(t_3) - \theta_3$ that still satisfies $\mu_3 \in (-\mu_s, 0)$.

Proof: As shown earlier, $\mu_0 > 0$ implies $\dot{\theta}_0 < 0$. From the proof of Lemma 2, recall that, at the end of the first phase, $\mu(t_2) = 0$ and $\dot{\theta}(t_2) = 0$. Due to the term $B\text{sgn}(\dot{\theta}_0)$ in a_P with $B > 0$ at $t = t_2$, $\dot{\alpha}_P(t_2) < 0$ and $\dot{\mu}(t_2) < 0$ following Eq. (15). Following similar arguments as in the discussion preceding Observation 3, at any time during the second phase, μ should be negative to achieve $\alpha^d_{P_f} \in [\theta_0, \pi + \theta_0)$. Note that $\mu(t_2) = 0$ and $\dot{\mu}(t_2) < 0$ imply $\dot{\theta}(t_2^+) > 0$. Therefore, starting with the initial condition of the second phase $\mu(t_2) = 0$ and $\dot{\mu}(t_2) < 0$, the condition for negative $\dot{\mu}$ follows from a_P in Lemma 3 and Eq. (15) as

$$(N - 1)|\dot{\theta}| - B/V_P < 0 \Rightarrow B > ((N - 1)V_P^2/R)\sin|\mu|; \qquad t > t_2 \tag{19}$$

It can be noted that many bias profiles B satisfying Eq. (19) and the integrable over time $t \geq t_2$ could be obtained for $R > 0$ [45]. Condition (19) leads to a monotonic decrease in μ starting from zero, which in effect implies $\dot{\theta} > 0$ for $t > t_2$, following Eq. (2). This implies that there exists a finite time $t_3 > t_2$ such that $\theta(t_3) = \theta_3 \in (\theta_2, \alpha^d_{P_f})$. Therefore, the inequality [Eq. (19)] can be written as

$$(N - 1)V_P(\theta(t) - \theta_2) < \int_{t_2}^{t} B\,\text{d}t; \qquad \forall t \in (t_2, t_3] \tag{20}$$

Thus, the right-hand side of inequality (20) is lower bounded. Also, from Eq. (15), the look-angle constraint for $t \in (t_2, t_3]$ can be written as

$$0 > \mu(t) > -\mu_s \Rightarrow (N - 1)V_P(\theta(t) - \theta_2) + V_P\mu_s > \int_{t_2}^{t} B\,\text{d}t; \quad \forall t \in (t_2, t_3] \tag{21}$$

Because $\mu_s > 0$, Eq. (21) provides an upper bound of the time integral of bias. Hence, Eqs. (20) and (21) imply the existence of a time-integrable bounded bias profile B [45], and hence a BPPN guidance law stated in Lemma 3. □

It can be noted from Eqs. (20) and (21) that there can be uncountably many integrable bias profiles that satisfy these conditions [45]. At $t = t_3$, these conditions imply

$$(N-1)V_P(\theta_3-\theta_2) < \int_{t_2}^{t_3} B\,\mathrm{d}t < (N-1)V_P(\theta_3-\theta_2) + V_P\mu_s \tag{22}$$

Among all those possible B profiles, a specific candidate function could be chosen in accordance with the following observation, where $B > 0$ is considered for a certain time interval during the second phase such that $\alpha_{P_f}^d \in (\theta_3, \pi+\theta_3]$ and Eq. (22) are satisfied at the end of the second phase.

Observation 7: For $\alpha_{P_0} > \theta_0$, during time $t \geq t_2$ in the second phase, a potential look-angle-constrained BPPN guidance command, satisfying Lemma 3, can be stated as follows:

1) $N < 1$ and bias $B > 0$ as long as LOS angle $\theta < \alpha_{P_f}^d$ and satisfies

$$(N-1)V_P(\theta-\theta_2) < \int_{t_2}^{t} B\,\mathrm{d}t < (N-1)V_P(\theta-\theta_2) + V_P\mu_s$$

Let until time $t = \hat{t}$, $\theta(\hat{t}) = \hat{\theta}$, and $\alpha_P(\hat{t}) = \hat{\alpha}_P$.

2) If $\alpha_{P_f}^d \in (\hat{\theta}, \hat{\theta}+\pi]$, then the second phase ends with $t_3 = \hat{t}$, $\alpha_{P_3} = \hat{\alpha}_P$, and $\theta_3 = \hat{\theta}$.

3) If $\hat{\theta} < -\pi + \alpha_{P_f}^d$, then use $N = 1$ and $B = 0$ until θ increases to a value θ_3 at some time $t_3 > \hat{t}$ such that $\alpha_{P_f}^d \in (\theta_3, \theta_3+\pi]$ [recall from Eqs. (19) and (2) that $N = 1$ and $B = 0$ implies $\dot{\mu} = 0$, and $\dot{\theta} > 0$ because μ remains a negative constant]. The second phase ends at time t_3 with $\alpha_P(t_3) = \alpha_{P_3}$.

Thus, Observation 7 describes a feasible computationally inexpensive, and hence real-time-implementable, bias-shaping method for the BPPN guidance in the second phase for satisfying look-angle constraints while leading to the final phase of the approach angle-constrained engagement. Now, BPPN in Lemma 2 for the first phase is combined with BPPN in Lemma 3 for the second phase to form the following three-phase bias-shaped composite guidance scheme for the look-angle-constrained approach angle control in the interval $[\theta_0, \pi+\theta_0)$.

Theorem 5: Consider $\alpha_{P_0} > \theta_0$. Use the look-angle-constrained bias-shaped BPPN, a combination of BPPN in Lemma 2 for the first phase, and BPPN in Lemma 3 and Observation 7 for the second phase, followed by PPN or look-angle-constrained 2pPPN, as mentioned in Observation 6, any $\alpha_{P_f}^d \in [\theta_0, \pi+\theta_0)$ can be achieved while still satisfying the FOV constraint.

Proof: Note that using look-angle-constrained bias-shaped BPPN for $\alpha_{P_0} > \theta_0$, an engagement condition $(\alpha_P, \theta) = (\alpha_{P_3}, \theta_3)$ is obtained at the end of the second phase such that $\alpha_{P_f}^d \in (\theta_3, \pi+\theta_3]$, and $0 > \mu_3 = \alpha_{P_3} - \theta_3 > -\mu_s$ (which follow from Lemmas 2, 3, and Observation 7). Hence, following Observation 6, $\alpha_{P_f}^d \in (\theta_3, 2\theta_3 - \alpha_{P_3}]$ can be achieved using PPN with $N = (\alpha_{P_f}^d - \alpha_{P_3})/(\alpha_{P_f}^d - \theta_3) \geq 2$, whereas $\alpha_{P_f}^d \in (2\theta_3 - \alpha_{P_3}, \pi+\theta_3]$ can be achieved using look-angle-constrained 2pPPN with $N = 1$ when $\theta \in [\theta_3, \alpha_{P_f}^d + \mu_3/(N_s-1))$, and $N = N_s$ otherwise, for some $N_s \geq 2$. □

An example of the look-angle-constrained trajectory generated by the three-phase composite guidance strategy of Theorem 5 is shown in Fig. 3b for achieving $\alpha_{P_f}^d = 5\pi/6$.

Observation 8: Following similar arguments as before, for $\alpha_{P_0} < \theta_0$ also it can be shown that using the look-angle-constrained bias-shaped BPPN guidance law, as given in Lemma 2 for the first phase, and a gain and bias profile similar to Lemma 3 and Observation 7, satisfying $B > 0$ as long as $\theta > \alpha_{P_f}^d$ and

$$(N-1)V_P(\theta_2-\theta) < \int_{t_2}^{t} B\,\mathrm{d}t < (N-1)V_P(\theta_2-\theta) + V_P\mu_s$$

during the second phase, followed by PPN or look-angle-constrained 2pPPN, as mentioned in Theorem 4, any $\alpha_{P_f}^d \in (-\pi+\theta_0, \theta_0]$ can be achieved.

C. $\mu\alpha$CIG Law and Algorithm

Based on the results presented in Secs. III.A and III.B, the all-approach-angle look-angle-constrained bias-shaped guidance law $\mu\alpha$CIG can be formulated as in the following theorem.

Theorem 6: Using PPN or look-angle-constrained 2pPPN, given in Theorem 4 and Observation 6, or the look-angle-constrained three-phase bias-shaped composite guidance strategy given in Theorem 5 and Observation 8, for $\alpha_{P_0} > \theta_0$ and $\alpha_{P_0} < \theta_0$, respectively, a full circle approach angle set $[-\pi, \pi)$ can be achieved while satisfying the FOV constraint.

Proof: The proof follows from Theorems 4 and 5 for $\alpha_{P_0} > \theta_0$ and Observations 6 and 8 for $\alpha_{P_0} < \theta_0$. □

Considering Theorems 4–6 and Observations 6–8, the $\mu\alpha$CIG algorithm can now be formulated as follows.

Given α_{P_0} and $\alpha_{P_f}^d$,

1) Use BPPN, $a_P^{\mu\alpha CIG} = NV_P\dot{\theta} + B\mathrm{sgn}(\dot{\theta})$ with $N = 2$ and B finite and positive until time t_1, at which $|\mu|$ becomes just less than μ_s if $|\mu_0| = |\alpha_{P_0} - \theta_0| \in (\mu_s, \pi)$. Let $\alpha_P(t_1) = \alpha_{P_1}$ and $\theta(t_1) = \theta_1$. Else if $|\mu_0| \in (0, \mu_s)$, then $t_1 = t_0$, $\alpha_P(t_1) = \alpha_{P_1} = \alpha_{P_0}$, and $\theta(t_1) = \theta_1 = \theta_0$.

2) Use PPN, $a_P^{\mu\alpha CIG} = NV_P\dot{\theta}$ with $N = (\alpha_{P_f}^d - \alpha_{P_1})/(\alpha_{P_f}^d - \theta_1)$ if $\alpha_{P_f}^d \in [2\theta_1 - \alpha_{P_1}, \theta_1)$ or $\alpha_{P_f}^d \in (\theta_1, 2\theta_1 - \alpha_{P_1}]$ for $\alpha_{P_1} > \theta_1$ or $\alpha_{P_1} < \theta_1$, respectively.

3) Use look-angle-constrained 2pPPN, $a_P^{\mu\alpha CIG} = NV_P\dot{\theta}$ with $N = 1$ for $\theta \in (\alpha_{P_f}^d + \mu_1/(N_s-1), \theta_1]$ or $\theta \in [\theta_1, \alpha_{P_f}^d + \mu_1/(N_s-1))$ for some $N_s \geq 2$, and use $N = N_s$ otherwise, if $\alpha_{P_f}^d \in [-\pi + \theta_1, 2\theta_1 - \alpha_{P_1})$ or $\alpha_{P_f}^d \in (2\theta_1 - \alpha_{P_1}, \pi + \theta_1]$ for $\alpha_{P_1} > \theta_1$ or $\alpha_{P_1} < \theta_1$, respectively.

4) Else, use the proposed three-phase look-angle-constrained bias-shaped composite guidance scheme:

a) In the first phase, use the BPPN guidance $a_P^{\mu\alpha CIG} = NV_P\dot{\theta} + B\mathrm{sgn}(\dot{\theta}_1)$ with $N = 2$ and $B > 0$ until $\dot{\theta}$ changes sign. When $\dot{\theta}$ crosses zero, let time $t = t_2$, $\theta = \theta_2$, and $\alpha_P = \alpha_{P_2}$; then, start the second phase as in Step 4b.

b) In the second phase, use the look-angle-constrained bias-shaped BPPN guidance $a_P^{\mu\alpha CIG} = NV_P\dot{\theta} + B\mathrm{sgn}(\dot{\theta}_1)$ with $N < 1$ and $B > 0$ at time $t \geq t_2$ as long as $\theta < \alpha_{P_f}^d$ and

$$(N-1)V_P(\theta-\theta_2) < \int_{t_2}^{t} B\,\mathrm{d}t < (N-1)V_P(\theta-\theta_2) + V_P\mu_s,$$

or $\theta > \alpha_{P_f}^d$ and

$$(N-1)V_P(\theta_2-\theta) < \int_{t_2}^{t} B\,\mathrm{d}t < (N-1)V_P(\theta_2-\theta) + V_P\mu_s$$

for $\alpha_{P_1} > \theta_1$ or $\alpha_{P_1} < \theta_1$, respectively; let up to time $\hat{t}$, $\theta(\hat{t}) = \hat{\theta}$, and $\alpha_P(\hat{t}) = \hat{\alpha}_P$.

i) If $\alpha_{P_f}^d \in (\hat{\theta}, \hat{\theta}+\pi]$ or $\alpha_{P_f}^d \in [-\pi+\hat{\theta}, \hat{\theta})$ for $\alpha_{P_1} > \theta_1$ or $\alpha_{P_1} < \theta_1$, respectively, then $t_3 = \hat{t}$, $\alpha_{P_3} = \hat{\alpha}_P$, and $\theta_3 = \hat{\theta}$. Start the third phase as in Step 4c.

ii) Continue the look-angle-constrained BPPN guidance $a_P^{\mu\alpha CIG} = NV_P\dot{\theta} + B\mathrm{sgn}(\dot{\theta}_1)$ with $N = 1$ and $B = 0$ until $\theta = \theta_3$ at some time t_3 such that $\alpha_{P_f}^d \in (\theta_3, \theta_3+\pi]$ or $\alpha_{P_f}^d \in [-\pi+\theta_3, \theta_3)$, if $\hat{\theta} < -\pi + \alpha_{P_f}^d$ or $\hat{\theta} > \pi + \alpha_{P_f}^d$ for $\alpha_{P_1} > \theta_1$ or $\alpha_{P_1} < \theta_1$, respectively. Let $\alpha_P(t_3) = \alpha_{P_3}$. At time $t = t_3$, start the third phase as in Step 4c.

c) Use PPN $a_P^{\mu\alpha CIG} = NV_P\dot{\theta}$ with $N = (\alpha_{P_f}^d - \alpha_{P_3})/(\alpha_{P_f}^d - \theta_3)$ if $\alpha_{P_f}^d \in (\theta_3, 2\theta_3 - \alpha_{P_3}]$ or $\alpha_{P_f}^d \in [2\theta_3 - \alpha_{P_3}, \theta_3)$ for $\alpha_{P_1} > \theta_1$ or $\alpha_{P_1} < \theta_1$, respectively.

d) Use look-angle-constrained 2pPPN $a_P^{\mu\alpha CIG} = NV_P\dot{\theta}$ with $N = 1$ for $\theta \in [\theta_3, \alpha_{P_f}^d + \mu_3/(N_s-1))$ or $\theta \in (\alpha_{P_f}^d + \mu_3/(N_s-1), \theta_3]$ for some $N_s \geq 2$, and $N = N_s$ otherwise, if $\alpha_{P_f}^d \in (2\theta_3 - \alpha_{P_3}, \pi + \theta_3]$ or $\alpha_{P_f}^d \in [-\pi + \theta_3, 2\theta_3 - \alpha_{P_3})$ for $\alpha_{P_1} > \theta_1$ or $\alpha_{P_1} < \theta_1$, respectively.

IV. All-Aspect Approach in 3-D

So far, only 2-D engagements were addressed. However, in practice, path-planning and motion control missions for UAVs are

conducted in a 3-D space, where an all-approach-angle approach implies an approach along any vector in the 3-D space. A usual approach to achieve this goal is to decouple engagement dynamics into mutually orthogonal yaw and pitch planes, and then control the vehicle in each plane separately. However, because engagement dynamics is essentially coupled, this approach leads to poorer performance in terms of the required control effort with respect to the approach, which takes into account coupled dynamics [24]. Therefore, to achieve the all-aspect approach in 3-D space, the integrated guidance schemes proposed for an all-aspect approach at a stationary target in a planar pursuit, presented in Secs. II.D and III.C, would be extended to a 3-D engagement, leaving aside any consideration of aforementioned decoupling. Thus, this approach provides a more realistic way to deal with this problem. Specifically, this section expands on the $\mu\alpha$CIG strategy to present the major result on a two-plane-segregated motion planning strategy to enable the UAV approaching a stationary target from any spatial direction, starting from any spatial direction, and still obeying FOV limitations.

A. 3-D Engagement Geometry

Consider a 3-D engagement geometry in which the UAV P, modeled as a point mass with a velocity vector $\boldsymbol{v}_P$, approaches a stationary target T, as shown in Fig. 4. In this figure, $\boldsymbol{r}_P$ and $\boldsymbol{r}_T$ denote the UAV and target position vectors, respectively; and $\boldsymbol{r} \triangleq \boldsymbol{r}_T - \boldsymbol{r}_P$ is the LOS vector between them. The initial and desired final velocity vectors of the UAV are given by $\boldsymbol{v}_{P_0}$ and $\boldsymbol{v}^d_{P_f}$, respectively. Using the LOS-fixed coordinate frame defined by three orthogonal unit vectors $\boldsymbol{e}_r$, $\boldsymbol{e}_t(\triangleq \dot{\boldsymbol{e}}_r/\omega)$, and $\boldsymbol{e}_\Omega(\triangleq \boldsymbol{\Omega}/\omega)$ [31,46], where $\boldsymbol{e}_r$ is the unit vector along the LOS, $\boldsymbol{\Omega} = R^{-1}\boldsymbol{e}_r \times (-\boldsymbol{v}_P) = \omega \boldsymbol{e}_\Omega$ is the angular velocity vector of the LOS, and $R = \|\boldsymbol{r}\|$, the dynamics of 3-D engagement can be expressed as follows:

$$
\begin{aligned}
&\boldsymbol{r} \triangleq R\boldsymbol{e}_r \triangleq \boldsymbol{r}_T - \boldsymbol{r}_P;\\
&\dot{\boldsymbol{r}} = \dot{R}\boldsymbol{e}_r + R\dot{\boldsymbol{e}}_{\boldsymbol{r}} = \dot{R}\boldsymbol{e}_r + R(\Omega \times \boldsymbol{e}_r) = -\boldsymbol{v}_P = -V_P(\boldsymbol{e}_P);\\
&\ddot{\boldsymbol{r}} = \ddot{R}\boldsymbol{e}_r + 2\dot{R}\dot{\boldsymbol{e}}_{\boldsymbol{r}} + R\ddot{\boldsymbol{e}}_{\boldsymbol{r}}\\
&\quad = (\ddot{R} - R\omega^2)\boldsymbol{e}_r + 2\dot{R}(\boldsymbol{\Omega} \times \boldsymbol{e}_r) + R(\dot{\boldsymbol{\Omega}} \times \boldsymbol{e}_r) = -\boldsymbol{a}_P
\end{aligned} \tag{23}
$$

$$
\boldsymbol{a}_{P_{PPN}} = NV_P(\boldsymbol{\Omega} \times \boldsymbol{e}_P) = NV_P\omega[(\boldsymbol{e}_P^T\boldsymbol{e}_r)\boldsymbol{e}_t - (\boldsymbol{e}_P^T\boldsymbol{e}_t)\boldsymbol{e}_r] \tag{24}
$$

From Eqs. (23) and (24), it follows that $\boldsymbol{r}$, $\boldsymbol{v}_P$, and $\boldsymbol{a}_P$ lie in the ($\boldsymbol{e}_r$, $\boldsymbol{e}_T$) plane, which remains invariant throughout the engagement because $\mathrm{d}(\boldsymbol{e}_r \times \boldsymbol{e}_t)/\mathrm{d}t = 0$ is assured by PPN [31,46]. This plane, referred to as the "engagement plane" (EP), is defined by the initial engagement geometry as a plane formed by $\boldsymbol{e}_{r_0}$ and $\boldsymbol{e}_{P_0}$. Therefore, although any approach angle on the invariant EP using αCIG and $\mu\alpha$CIG strategies is feasible, not any approach vector $\boldsymbol{v}^d_{P_f}$ is achievable by them if $\boldsymbol{v}^d_{P_f}$ does not belong to the EP. To achieve any approach vector starting from any initial heading configuration of the UAV, a further expansion of the integrated guidance scheme developed in Sec. III is necessary.

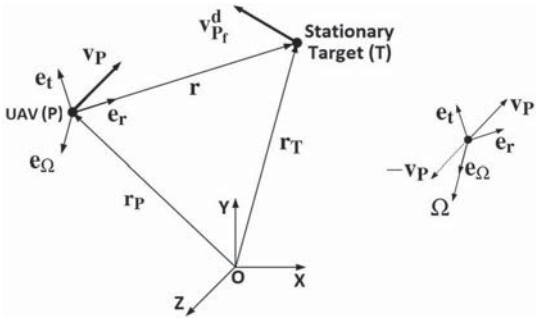

Fig. 4 3-D engagement geometry.

B. $\mu\alpha$CIG3D Background

In a generic 3-D engagement, the vectors $\boldsymbol{v}_{P_0}$, $\boldsymbol{r}_0$, and $\boldsymbol{v}^d_{P_f}$ are not coplanar. In this case, however, the entire 3-D engagement could be segmented into two planar phases, which take place in two different engagement planes, respectively. First, the UAV moves on the initial EP (EP_0) formed by $\boldsymbol{v}_{P_0}$ and $\boldsymbol{r}_0$, which means that at the end of the first planar phase, $\boldsymbol{r}$ and $\boldsymbol{v}_P$ can be represented as a linear combination of $\boldsymbol{e}_{P_0}$ and $\boldsymbol{e}_{r_0}$. Thus, $EP_0 \triangleq \mathrm{span}(\boldsymbol{e}_{P_0}, \boldsymbol{e}_{r_0})$. The EP for the second planar-phase EP_f should contain $\boldsymbol{v}^d_{P_f}$, meaning that $\boldsymbol{v}_P$ at the beginning of the second planar phase should be a linear combination of $\boldsymbol{r}$ at the end of the first planar phase and $\boldsymbol{v}^d_{P_f}$. These two factors imply that $\boldsymbol{r}$ and $\boldsymbol{v}_P$ at the end of the first planar phase should be aligned. This condition might be achieved in many different ways, leading to different $\boldsymbol{r}$ at the end of the first planar phase. One such scheme is when, in the second planar phase, the UAV is guided on the final EP formed by $\boldsymbol{v}^d_{P_f}$ and $\boldsymbol{r}_0$. Thus, $EP_f \triangleq \mathrm{span}(\boldsymbol{e}^d_{P_f}, \boldsymbol{e}_{r_0})$. These two EPs are depicted in Fig. 5. The advantage of this approach is that two EPs can easily be predecided by the initial and desired terminal geometries, whereas the line of intersection between these two EPs lies along $\boldsymbol{r}_0$. A schematic trajectory generated using this two-plane-segregated guidance strategy is depicted in Fig. 5. Now, consider a point called a "virtual target" (VT) $\boldsymbol{r}_{VT}$ as

$$
\boldsymbol{r}_{VT} = \boldsymbol{r}_{P_0} + \beta \boldsymbol{r}_0, \beta \in (0, 1] \tag{25}
$$

Because EP_0 is formed by $\boldsymbol{v}_{P_0}$ and $\boldsymbol{r}_0$, a velocity heading along the direction of $\boldsymbol{r}_0$ at VT on EP_0 can be achieved using the look-angle-constrained bias-shaped composite guidance strategy presented in Step 4 of the $\mu\alpha$CIG algorithm in Sec. III.C. Similarly, because EP_f is formed by $\boldsymbol{v}^d_{P_f}$ and $\boldsymbol{r}_0$, starting from $\boldsymbol{v}_P$ along $\boldsymbol{e}_{r_0}$ at the VT, the UAV could be guided on the EP_f plane by the $\mu\alpha$CIG strategy to achieve the desired approach vector $\boldsymbol{v}^d_{P_f}$ as well. Realization of this two-plane-segregated strategy ($\mu\alpha$CIG3D) requires $\boldsymbol{r}_{VT}$ to be sufficiently away from both $\boldsymbol{r}_{P_0}$ and $\boldsymbol{r}_T$ such that the UAV gets sufficient space for necessary turning in the first and second planar phases, respectively. This indicates that β should be neither too high nor too low.

It should be noted that, instead of a two-plane-segmented scheme, a multiplane-segmented scheme could also have been implemented. Such multiplane-segmented schemes could be of relevance in the case of problem-specific motion planning of UAVs. Such a multiplane-segregated scheme would still have EP_0 spanned by $\boldsymbol{e}_{P_0}$ and $\boldsymbol{e}_{r_0}$, and EP_f spanned by $\boldsymbol{e}^d_{P_f}$ and $\boldsymbol{e}_r$ at the end of last but one planar phase. The transition from one planar phase to the next one could be performed in a manner similar to the two-planar-phase scheme addressed in more detail next.

C. First Planar Phase of $\mu\alpha$CIG3D

By construction of the VT as in Eq. (25), it lies on the initial LOS that is in the $\boldsymbol{e}_{r_0}$ direction with respect to the UAV's initial position $\boldsymbol{r}_{P_0}$. Consider an LOS-fixed reference frame, ($\boldsymbol{e}_{r_{p1}}$, $\boldsymbol{e}_{t_{p1}}$, $\boldsymbol{e}_{\Omega_{p1}}$) as described in Sec. IV.A, where $\boldsymbol{e}_{r_{P1}}$ is the unit vector along the LOS between the UAV and the VT. Note that the magnitude of angular

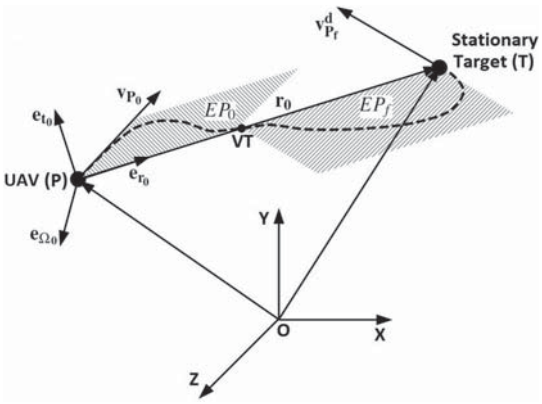

Fig. 5 UAV's trajectory in a two-plane-segregated engagement.

velocity of the LOS vector $\boldsymbol{\Omega}$ is nonnegative. A positive ω_0 implies that UAV's initial heading angle is less than the initial LOS angle on the EP_0 plane; that is,

$$\begin{aligned}\alpha_{P_{p1_0}} &= \tan^{-1}\left(\boldsymbol{e}_{P_0}\cdot\boldsymbol{e}_{t_{p1_0}}/\boldsymbol{e}_{P_0}\cdot\boldsymbol{e}_{r_0}\right)\\ &< \theta_{p1_0} = \tan^{-1}\left(\boldsymbol{e}_{r_{p1_0}}\cdot\boldsymbol{e}_{t_{p1_0}}/\boldsymbol{e}_{r_{p1_0}}\cdot\boldsymbol{e}_{r_0}\right)=0\end{aligned}$$

where the $\tan^{-1}$ function is considered to map a real number to an interval of $[-\pi, \pi)$.

Consider $\boldsymbol{e}_{P_0}\neq\pm\boldsymbol{e}_{r_0}$. Note that $\alpha_{P_f}\in(\theta_0, \pi+\theta_0]$ in the case of planar engagement with $\alpha_{P_0}\in[-\pi+\theta_0, \theta_0)$ corresponds to a hemisphere given by

$$\begin{aligned}\Big\{\{-\boldsymbol{e}_{r_0}\}, \{\boldsymbol{e}_{P_f}\neq\pm\boldsymbol{e}_{r_0}|\boldsymbol{e}_{r_0}\times\boldsymbol{e}_{P_0}/\|\boldsymbol{e}_{r_0}\times\boldsymbol{e}_{P_0}\|\\ =-\boldsymbol{e}_{r_0}\times\boldsymbol{e}_{P_f}/\|\boldsymbol{e}_{r_0}\times\boldsymbol{e}_{P_f}\|\}\Big\}\end{aligned}$$

in the case of 3-D engagement. For planar engagements, the VT coincides with the actual stationary target (that is, $\beta=1$), and the engagement ends with this planar phase only with $\boldsymbol{e}^d_{P_{P1_f}}=\boldsymbol{e}^d_{P_f}$, which can be achieved by using $\mu\alpha$CIG as discussed in Sec. III.C. However, for nonplanar engagements, $\boldsymbol{e}^d_{P_{P1_f}}$ is aligned with $\boldsymbol{e}_{r_0}$, which implies that, at the end of the first planar phase in the EP_0 plane,

$$\alpha^d_{P_{p1_f}}=\tan^{-1}\left(\boldsymbol{e}^d_{P_{P1_f}}\cdot\boldsymbol{e}_{t_0}/\boldsymbol{e}^d_{P_{P1_f}}\cdot\boldsymbol{e}_{r_0}\right)=0$$

This can be achieved using the look-angle-constrained bias-shaped three-phase composite guidance scheme described in Step 4 of the $\mu\alpha$CIG strategy in Sec. III.C. Thus, the look-angle-constrained integrated guidance algorithm for the first planar phase, which consists of the first three phases of the overall $\mu\alpha$CIG3D for controlling approach vector in 3-D engagement, can be formulated as follows:

1) Initialize with the UAV's position $\boldsymbol{r}_{P_0}$ and velocity vector $\boldsymbol{v}_{P_0}$, as well as the target's position $\boldsymbol{r}_T$. Obtain the initial range vector $\boldsymbol{r}_0=\boldsymbol{r}_T-\boldsymbol{r}_{P_0}$, $EP_0=\text{span}(\boldsymbol{v}_{P_0}, \boldsymbol{r}_0)$, $\boldsymbol{r}_{VT}=\boldsymbol{r}_{P_0}+\beta\boldsymbol{r}_0$ for $\beta\in(0, 1]$, and define the reference frame

$$\left\{\boldsymbol{e}_{r_{p1_0}}, \boldsymbol{e}_{t_{p1_0}}, \boldsymbol{e}_{\Omega_{p1_0}}\right\}$$

reference frame as

$$\begin{aligned}\boldsymbol{e}_{r_{p1_0}} &= (\boldsymbol{r}_{VT}-\boldsymbol{r}_{P_0})/\|\boldsymbol{r}_{VT}-\boldsymbol{r}_{P_0}\|=\boldsymbol{e}_{r_0}\\ \boldsymbol{e}_{t_{p1_0}} &(\triangleq \dot{\boldsymbol{e}}_{r_{p1_0}}/\omega_{p1_0})\\ \boldsymbol{e}_{\Omega_{p1_0}} &(\triangleq \boldsymbol{\Omega}_{p1_0}/\omega_{p1_0})\end{aligned}$$

where

$$\boldsymbol{\Omega}_{p1_0}=R^{-1}_{VT_0}\boldsymbol{e}_{r_{p1_0}}\times(-\boldsymbol{v}_{P_0})=\omega_{p1_0}\boldsymbol{e}_{\Omega_{p1_0}}$$

Compute the UAV's initial heading angle

$$\alpha_{P_{p1_0}}=\tan^{-1}\left(\boldsymbol{e}_{P_0}\cdot\boldsymbol{e}_{t_{p1_0}}/\boldsymbol{e}_{P_0}\cdot\boldsymbol{e}_{t_{p1_0}}\right)$$

and initial LOS angle with respect to the VT as

$$\theta_{p1_0}=\tan^{-1}\left(\boldsymbol{e}_{r_{VT}}\cdot\boldsymbol{e}_{t_{p1_0}}/\boldsymbol{e}_{r_{VT}}\cdot\boldsymbol{e}_{r_{p1_0}}\right)=0$$

on the EP_0 plane, and the desired approach angle at the VT as

$$\alpha^d_{P_{p1_f}}=\tan^{-1}\left(\boldsymbol{e}^d_{P_{p1_f}}\cdot\boldsymbol{e}_{t_{p1_0}}/\boldsymbol{e}^d_{P_{p1_f}}\cdot\boldsymbol{e}_{r_{p1_0}}\right)$$

2) Use BPPN

$$\boldsymbol{a}^{\mu\alpha CIG3D}_{P_{p1}}=\left(NV_P\omega_{p1}+B\right)\left(\boldsymbol{e}_{\Omega_{p1}}\times\boldsymbol{e}_P\right)$$

with $N=2$ and B finite positive until time t_1, at which $|\mu_{p1}|$ becomes just less than μ_s if $\mu_{p1_0}=\alpha_{P_{p1_0}}-\theta_{p1_0}\in(-\pi, -\mu_s]$. Note that $\boldsymbol{e}_{\Omega_{P1}}(t_1)=\boldsymbol{e}_{\Omega_{P1_0}}$. Let $\alpha_{P_{p1}}(t_1)=\alpha_{P_1}$ and $\theta_{p1}(t_1)=\theta_1$. Otherwise, if $\mu_{p1_0}\in(-\mu_s, 0)$, then $t_1=t_0$, $\alpha_{P_{p1}}(t_1)=\alpha_{P_1}=\alpha_{P_0}$, and $\theta_{p1}(t_1)=\theta_1=\theta_0$. If the engagement is planar, go to Step 3; else, go to Step 5.

3) (Applicable for planar engagements only) Use PPN

$$\boldsymbol{a}^{\mu\alpha CIG3D}_{P_{p1}}=NV_P\omega_{p1}\left(\boldsymbol{e}_{\Omega_{p1}}\times\boldsymbol{e}_P\right)$$

with $N=(\alpha^d_{P_{p1_f}}-\alpha_{P_1})/(\alpha^d_{P_{p1_f}}-\theta_1)$ if $\alpha^d_{P_{p1_f}}\in(\theta_1, 2\theta_1-\alpha_{P_1}]$.

4) (Applicable for planar engagements only) Use look-angle-constrained 2pPPN

$$\boldsymbol{a}^{\mu\alpha CIG3D}_{P_{p1}}=NV_P\omega_{p1}\left(\boldsymbol{e}_{\Omega_{p1}}\times\boldsymbol{e}_P\right)$$

with $N=1$ for $\theta\in[\theta_1, \alpha^d_{P_{p1_f}}+\mu_1/(N_s-1))$ for some $N_s\geq 2$, and $N=N_s$ otherwise, if $\alpha^d_{P_{p1_f}}\in(2\theta_1-\alpha_{P_1}, \pi+\theta_1]$. Or else, go to Step 5.

5) Use Step 4 of the $\mu\alpha$CIG scheme as follows:

a) In the first phase, use the BPPN guidance

$$\boldsymbol{a}^{\mu\alpha CIG3D}_{P_{p1}}=\left(NV_P\omega_{p1}+B\right)\left(\boldsymbol{e}_{\Omega_{p1}}\times\boldsymbol{e}_P\right)$$

with $N=2$ and bias $B>0$ until $\boldsymbol{e}_{\Omega_{P1}}$ reverses direction; let, at time $t=t_2$, $\alpha_{P_{p1}}(t_2)=\alpha_{P_2}$ and $\theta_{p1}(t_2)=\theta_2$. At time t_2, start the second phase as in Step 5b.

b) In the second phase, use the look-angle-constrained bias-shaped BPPN guidance

$$\boldsymbol{a}^{\mu\alpha CIG3D}_{P_{p1}}=NV_P\omega_{p1}\left(\boldsymbol{e}_{\Omega_{p1}}\times\boldsymbol{e}_P\right)+B\left(\boldsymbol{e}_{\Omega_{p1_0}}\times\boldsymbol{e}_P\right)$$

with $N<1$ and $B>0$ at time $t\geq t_2$ as long as $\theta_{p1}>\alpha^d_{P_{p1_f}}$ and

$$(N-1)V_P(\theta_2-\theta_{p1})<\int_{t_2}^{t}B\,\mathrm{d}t<(N-1)V_P(\theta_2-\theta_{p1})+V_P\mu_s,$$

let up to time $\hat{t}$, $\theta_{p1}(\hat{t})=\hat{\theta}_{p1}$ and $\alpha_{P_{p1}}(\hat{t})=\hat{\alpha}_{P_{p1}}$.

i) If $\alpha^d_{P_{p1_f}}\in[-\pi+\hat{\theta}_{p1}, \hat{\theta}_{p1})$, then $t_3=\hat{t}$, $\alpha_{P_3}=\hat{\alpha}_{P_{p1}}$, and $\theta_3=\hat{\theta}_{p1}$. Start the third phase as in Step 5c.

ii) Continue the look-angle-constrained BPPN guidance

$$\boldsymbol{a}^{\mu\alpha CIG3D}_{P_{p1}}=NV_P\omega_{p1}\left(\boldsymbol{e}_{\Omega_{p1}}\times\boldsymbol{e}_P\right)+B\left(\boldsymbol{e}_{\Omega_{p1_0}}\times\boldsymbol{e}_P\right)$$

with $N=1$ and $B=0$ until $\theta_{p1}=\theta_3$ at some time t_3 such that $\alpha^d_{P_{p1_f}}\in[-\pi+\theta_3, \theta_3)$, if $\hat{\theta}_{p1}>\pi+\alpha^d_{P_f}$. Let $\alpha_{P_{p1}}(t_3)=\alpha_{P_3}$. At time $t=t_3$, start the third phase as in Step 5c.

c) Use PPN

$$\boldsymbol{a}^{\mu\alpha CIG3D}_{P_{p1}}=NV_P\omega_{p1}\left(\boldsymbol{e}_{\Omega_{p1}}\times\boldsymbol{e}_P\right)$$

with $N=(\alpha^d_{P_{p1_f}}-\alpha_{P_3})/(\alpha^d_{P_{p1_f}}-\theta_3)$, if $\alpha^d_{P_{p1_f}}\in[2\theta_3-\alpha_{P_3}, \theta_3]$.

d) Use look-angle-constrained 2pPPN

$$\boldsymbol{a}^{\mu\alpha CIG3D}_{P_{P1}}=NV_P\omega_{p1}(\boldsymbol{e}_{\Omega_{P1}}\times\boldsymbol{e}_P)$$

with navigation gain $N=1$ for

$$\theta_{p1}\in\left(\alpha^d_{P_{p1_f}}+\mu_s/(N_s-1), \theta_3\right]=(|\mu_3|/(N_s-1), \theta_3]$$

for some $N_s \geq 2$, and $N = N_s$ otherwise, if $\alpha^d_{P_{p1_f}} \in [-\pi + \theta_3, 2\theta_3 - \alpha_{P_3})$.

For $\boldsymbol{e}_{P_0} = \boldsymbol{e}_{r_0}$ or $\boldsymbol{e}_{P_0} = -\boldsymbol{e}_{r_0}$, which are equivalent to $\mu_0 = 0$ and $-\pi$, respectively, the engagement becomes planar. In these cases, a suitable adjustment pulse bias B_{adj}, similar to that described in Observation 2, needs to be applied at the beginning of the engagement to obtain an engagement geometry outside the collision or inverse collision course, respectively.

D. Second Planar Phase of $\mu\alpha$CIG3D

As the UAV reaches the VT along the $\boldsymbol{e}_{r_0}$ direction (that is, when $\boldsymbol{r}_P = \boldsymbol{r}^d_{P_{p1_f}} = \boldsymbol{r}_{VT}$ and $\boldsymbol{e}_P = \boldsymbol{e}^d_{P_{p1_f}} = \boldsymbol{e}_{r_0}$), the second planar phase of engagement commences in the EP_f plane. This planar phase begins with an LOS vector with respect to the stationary target along

$$\boldsymbol{e}_{r_{p2_0}} = \left(\boldsymbol{r}_T - \boldsymbol{r}^d_{P_{p1_f}}\right) / \left\|\boldsymbol{r}_T - \boldsymbol{r}^d_{P_{p1_f}}\right\| = \boldsymbol{e}_{r_0}$$

(see Fig. 5). At the beginning of this planar phase, $\boldsymbol{e}_{P_{p2_0}} = \boldsymbol{e}_{r_{p2_0}}$ implies that the UAV is on a collision course with the stationary target; therefore, $\omega_{p2_0} = 0$. This necessitates an alternative strategy to obtain an LOS-fixed reference frame at the beginning of this planar phase. Following the discussion in Sec. II.B for a PPN-guided UAV against a stationary target, the LOS angle θ and UAV's heading angle α_P converge to the same value at the time of final approach. In the case of the approach vector-constrained 3-D engagement scenario, this implies that $\boldsymbol{e}_{r_f} = \boldsymbol{e}^d_{P_f}$. So, in the second planar phase, $\boldsymbol{e}_r$ should rotate from $\boldsymbol{e}_{r_0}$ orientation to $\boldsymbol{e}^d_{P_f}$ orientation, which implies that the angular rotation vector of the LOS should be aligned with

$$\boldsymbol{e}_{\Omega_{p2}} = \boldsymbol{e}_{r_0} \times \boldsymbol{e}^d_{P_f} / \|\boldsymbol{e}_{r_0} \times \boldsymbol{e}^d_{P_f}\|$$

For the planar engagement in this planar phase on the EP_f plane, $\boldsymbol{e}_{\Omega_{P2}}$ is invariant with respect to rotations following the discussion in Sec. IV.A. Hence,

$$\boldsymbol{e}_{\Omega_{p2_0}} = \boldsymbol{e}_{r_0} \times \boldsymbol{e}^d_{P_f} / \|\boldsymbol{e}_{r_0} \times \boldsymbol{e}^d_{P_f}\|$$

and

$$\boldsymbol{e}_{t_{p2_0}} = \boldsymbol{e}_{\Omega_{p2_0}} \times \boldsymbol{e}_{r_0}$$

The UAV's heading angle and LOS angle with respect to the stationary target are given as

$$\alpha_{P_{p2}} = \tan^{-1}\left(\boldsymbol{e}_P \cdot \boldsymbol{e}_{t_{p2_0}} / \boldsymbol{e}_P \cdot \boldsymbol{e}_{r_{p2_0}}\right)$$

and

$$\theta_{p2} = \tan^{-1}\left(\boldsymbol{e}_{r_{p2}} \cdot \boldsymbol{e}_{t_{p2_0}} / \boldsymbol{e}_{r_{p2}} \cdot \boldsymbol{e}_{r_{p2_0}}\right)$$

respectively, where $\boldsymbol{e}_{r_{P2}}$ is the unit vector of the LOS vector between the UAV and the target. This leads to

$$\alpha^d_{P_{p2_f}} = \tan^{-1}\left(\boldsymbol{e}^d_{P_f} \cdot \boldsymbol{e}_{t_{p2_0}} / \boldsymbol{e}^d_{P_f} \cdot \boldsymbol{e}_{r_{p2_0}}\right) \in (0, \pi]$$

Also, note that

$$\alpha_{P_{p2_0}} = \theta_{p2_0} = 0$$

corresponding to a collision course. This calls for an adjustment bias at the beginning of the engagement similar to the one described in Observation 2. The adjustment bias can be described as

$$B_{\text{adj}} = b_{\text{adj}}(-\boldsymbol{e}_{\Omega_{p2}} \times \boldsymbol{e}_P)$$

where b_{adj} is a positive and finite number. This adjustment bias needs to be applied for a short interval such that, at the end of the application of this bias, θ_{p2} and $\alpha_{P_{p2}}$ satisfy

$$\alpha^d_{P_{p2_f}} = \tan^{-1}\left(\boldsymbol{e}^d_{P_f} \cdot \boldsymbol{e}_{t_{p2_0}} / \boldsymbol{e}^d_{P_f} \cdot \boldsymbol{e}_{r_{p2_0}}\right) \in (\theta_{p2}, \pi + \theta_{p2}]$$

and

$$|\mu_{p2}| = |\alpha_{P_{p2}} - \theta_{p2}| < \mu_s$$

These conditions ensure that the rest of the approach vector-constrained engagement in the EP_f plane could be achieved using PPN or look-angle-constrained 2pPPN only. As a result, the look-angle-constrained integrated guidance algorithm for the second planar phase comprising the fourth and fifth phases of the overall $\mu\alpha$CIG3D strategy for controlling the approach vector in 3-D engagement is given as follows:

1) Initialize with the UAV's position $\boldsymbol{r}_{P_{p2_0}} = \boldsymbol{r}_{VT}$ and velocity $\boldsymbol{v}_{P_{p2_0}} = V_P \boldsymbol{e}_{P_{p2_0}}$, where $\boldsymbol{e}_{P_{p2_0}} = \boldsymbol{e}_{r_{p2_0}} = \boldsymbol{e}_{r_0}$, and the target's position is $\boldsymbol{r}_T$. Obtain $EP_f = \text{span}(\boldsymbol{e}^d_{P_f}, \boldsymbol{e}_{r_0})$ and define the reference frame

$$\left\{\boldsymbol{e}_{r_{p2_0}}, \boldsymbol{e}_{t_{p2_0}}, \boldsymbol{e}_{\Omega_{p2_0}}\right\}$$

as

$$\boldsymbol{e}_{r_{p2_0}} = (\boldsymbol{r}_T - \boldsymbol{r}_{P_{p2_0}}) / \|\boldsymbol{r}_T - \boldsymbol{r}_{P_{p2_0}}\| = \boldsymbol{e}_{r_0}$$
$$\boldsymbol{e}_{\Omega_{p2_0}} = \boldsymbol{e}_{r_0} \times \boldsymbol{e}^d_{P_f} / \|\boldsymbol{e}_{r_0} \times \boldsymbol{e}^d_{P_f}\|$$

and

$$\boldsymbol{e}_{t_{p2_0}} = \boldsymbol{e}_{\Omega_{p2_0}} \times \boldsymbol{e}_{r_0}$$

Compute the UAV's initial heading

$$\alpha_{P_{p2_0}} = \tan^{-1}\left(\boldsymbol{e}_{P_{p2_0}} \cdot \boldsymbol{e}_{t_{p2_0}} / \boldsymbol{e}_{P_{p2_0}} \cdot \boldsymbol{e}_{r_{p2_0}}\right) = 0$$

and initial LOS angle with respect to the stationary target

$$\theta_{p2_0} = \tan^{-1}\left(\boldsymbol{e}_{r_T} \cdot \boldsymbol{e}_{t_{p2_0}} / \boldsymbol{e}_{r_T} \cdot \boldsymbol{e}_{r_{p2_0}}\right) = 0$$

on the EP_f plane and the desired approach angle at stationary target

$$\alpha^d_{P_{p2_f}} = \tan^{-1}\left(\boldsymbol{e}^d_{P_f} \cdot (\boldsymbol{e}_{t_{p2_0}}) / \boldsymbol{e}^d_{P_f} \cdot \boldsymbol{e}_{r_{p2_0}}\right) \in (0, \pi]$$

2) Use the look-angle-constrained two-phase composite guidance scheme as follows:

a) In the fourth phase, use a pulse adjustment bias guidance command

$$\boldsymbol{a}^{\mu\alpha CIG3D}_{P_{p2}} = b_{\text{adj}}\left(-\boldsymbol{e}_{\Omega_{p2_0}} \times \boldsymbol{e}_P\right)$$

as long as $\alpha_{P_{p2}}$ and θ_{p2} satisfy $\alpha^d_{P_{p2_f}} \in (0, \pi] \cap (\theta_{p2}, \pi + \theta_{p2}] = (\theta_{p2}, \pi]$ and $|\mu_{p2}| = |\alpha_{P_{p2}} - \theta_{p2}| < \mu_s$. Let at the end of the application of the adjustment bias be $t = t_5$, $\alpha_{P_{p2}}(t_5) = \alpha_{P_5}$, and $\theta_{p2}(t_5) = \theta_5$. Start the fifth phase at time t_5 as in Step 2b.

b) In the fifth phase, compute $\boldsymbol{\Omega}_{p2} = R^{-1}\boldsymbol{e}_{r_{p2}} \times (-\boldsymbol{v}_P) = \omega_{p2}\boldsymbol{e}_{\Omega_{p2}}$. Use PPN $\boldsymbol{a}^{\mu\alpha CIG3D}_{P_{p2}} = NV_P\omega_{p2}(\boldsymbol{e}_{\Omega_{p2}} \times \boldsymbol{e}_P)$ with $N = (\alpha^d_{P_{p2_f}} - \alpha_{P_5})/(\alpha^d_{P_{p2_f}} - \theta_5)$, if $\alpha^d_{P_{p2_f}} \in (\theta_5, 2\theta_5 - \alpha_{P_5}]$.

c) Use look-angle-constrained 2pPPN

$$\boldsymbol{a}^{\mu\alpha CIG3D}_{P_{p2}} = NV_P\omega_{p2}\left(\boldsymbol{e}_{\Omega_{p2}} \times \boldsymbol{e}_P\right)$$

with $N = 1$ for $\theta_{p2} \in [\theta_5, \alpha^d_{P_{p2_f}} - \mu_5/(N_s - 1))$ for some $N_s \geq 2$, and $N = N_s$ otherwise, if $\alpha^d_{P_{p2_f}} \in (2\theta_5 - \alpha_{P_5}, \pi]$.

Observation 9: The $\mu\alpha$CIG3D integrates two look-angle-constrained composite guidance algorithms (a three-phase scheme for the first planar phase and a two-phase scheme for the second planar phase) to achieve the all-aspect approach in a 3-D engagement. The first planar phase of $\mu\alpha$CIG3D follows the $\mu\alpha$CIG strategy, which ensures $\boldsymbol{e}_{P_{p1_f}} = \boldsymbol{e}^d_{P_{p1_f}} = \boldsymbol{e}_{r_0}$ from any initial heading of the UAV on the EP_0 plane, and the second planar phase of $\mu\alpha$CIG3D uses adjustment bias guidance with a suitable sign that helps in attaining such an engagement geometry from which PPN or FOV-constrained 2pPPN would be sufficient to achieve $\boldsymbol{e}^d_{P_f}$ on the EP_f plane. This along with the fact that the two engagement planes EP_0 and EP_f could easily be predecided by the initial and desired final geometries makes the $\mu\alpha$CIG3D strategy the least restrictive and thus suitable for all possible initial and desired terminal heading directions.

V. Computer Simulation Results

This section reviews the results of αCIG, $\mu\alpha$CIG, and $\mu\alpha$CIG3D simulations. These simulations assume the speed and maximum turn rate capacity of the UAV to be $V_P = 50$ m/s and $\|\dot{\boldsymbol{e}}_{P_{\max}}\| = \pi/4$ rad/s, respectively (corresponding to $\|\boldsymbol{a}_{P_{\max}}\| = V_P\|\dot{\boldsymbol{e}}_{P_{\max}}\| = 39.3\ \text{m/s}^2 \approx 4g$).

The FOV angle constraint is given by the UAV's threshold look angle $\mu_s = \pi/4$. All simulations are run on the Intel Core i7 3.20 GHz computer in the MATLAB development environment. The integration step of 0.05 s (corresponding to a 20 Hz command rate) is used for simulations. In the environment, the computation of a guidance command takes about 0.0002 s, meaning that there is no problem implementing developed algorithms on a real aircraft. In this and the following section, the time histories of angular quantities are shown in degrees in the simulation figures; whereas in the text, they are quantified in radians for better understanding.

A. 2-D Engagements Using αCIG and $\mu\alpha$CIG

The time histories of the UAV's trajectory, the look angle, the magnitude of the UAV's lateral acceleration, and the normalized bias profile in the UAV's lateral acceleration along with the phases for 2-D engagements with different values of $\alpha^d_{P_f}$ are shown in Figs. 6–8. The initial geometry was characterized by the UAV's heading angle of $\alpha_{P_0} = 3\pi/4$, the range of $R_0 = 2500$ m, and the LOS angle of $\theta_0 = 0$. Three desired final headings ($\alpha^d_{P_f}$) are 0, $\pi/3$, and $5\pi/6$, respectively.

Here, $\alpha_{P_0} \in [0, \pi)$, and $\alpha^d_{P_f} \in [0, \pi)$ in each of these three cases, meaning that neither PPN nor 2pPPN could be employed. Instead, all these cases use the αCIG strategy with the first phase initiated with $N = 2$ and a bias of $B = V_P|\alpha_P|/5$. Because $N > 1$ and $B > 0$, μ monotonically decreases; after some time, it falls within the $\mu < \mu_s$ limit. The first phase ends at a time of $t_2 = 27.05$ s, when $\dot{\theta}$ reverses its sign at $\theta = \theta_2 = -0.22$ rad (see Lemma 2).

In the second phase, $N = -2$ and $B = V_P|\alpha_P|/10$. Without the look-angle constraint, the second phase ends at $t_3 = 37.8$ s, when $\theta = \theta_3 = -0.072$ rad $\in (\theta_2, \theta_0] = (-0.22, 0]$ rad, and $\alpha_P = \alpha_{P_3} = -1.049$ rad. Note that each of the considered values of $\alpha^d_{P_f}$ is within the interval of $(\theta_3, \pi + \theta_3] = (-0.072, 3.07]$ rad. However, from the time histories of μ in Figs. 6b, 7b, and 8b, it is clearly seen that look angle falls below the FOV limit. To prevent it from happening, the bias-shaping method in Lemma 3 and Observation 7 is followed; thus, the second phase continues as long as $\theta < \alpha^d_{P_f}$ and $(N-1)(\theta - \theta_2) - \int_{t_2}^{t} (B/V_P)\,\mathrm{d}t + \mu_s$ remains positive. This leads to an earlier termination of the second phase in the look-angle-constrained scenario at a time of $t_3 = 36.9$ s, which is discernible from Figs. 6b, 6d, 7b, 7d, 8b, and 8d. This time, $\theta_3 = -0.109$ rad, which is also less than θ_3 in the case of a no-FOV constraint, and $\alpha_{P_3} = -0.89$ rad. However,

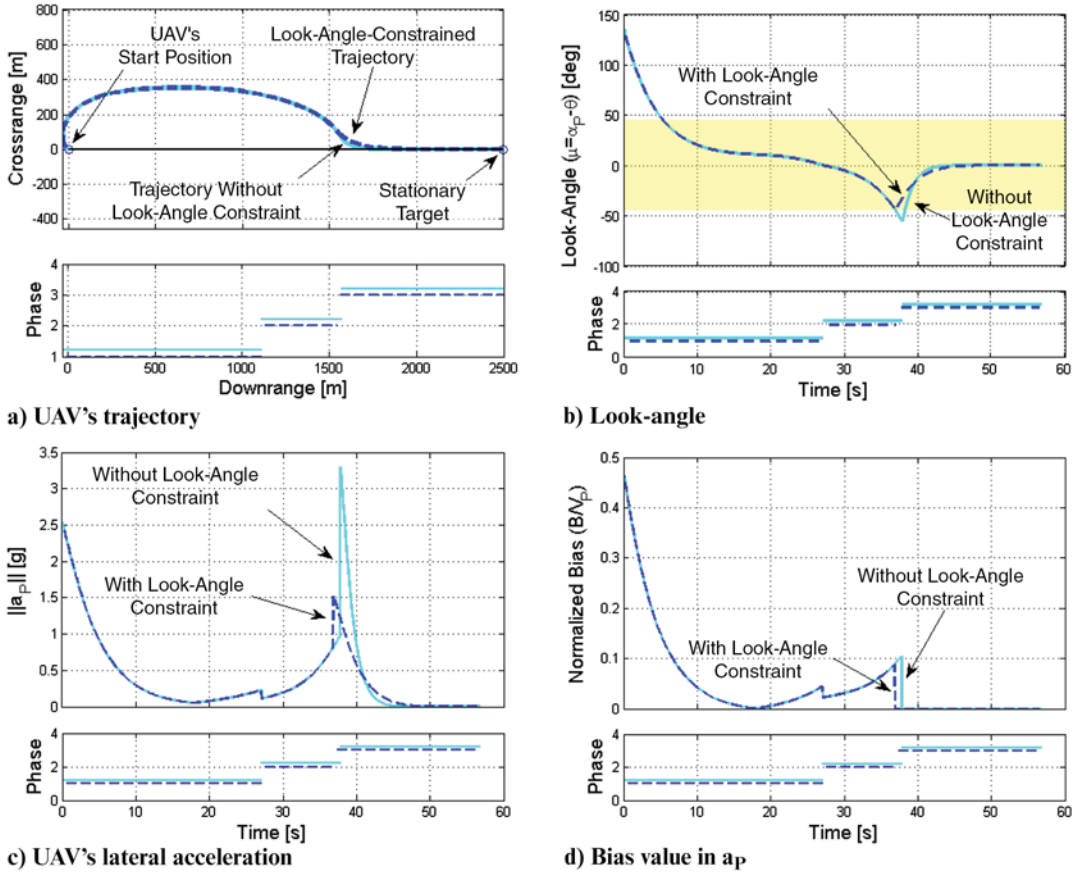

Fig. 6 2-D engagement with $\alpha^d_{P_f} = 0$.

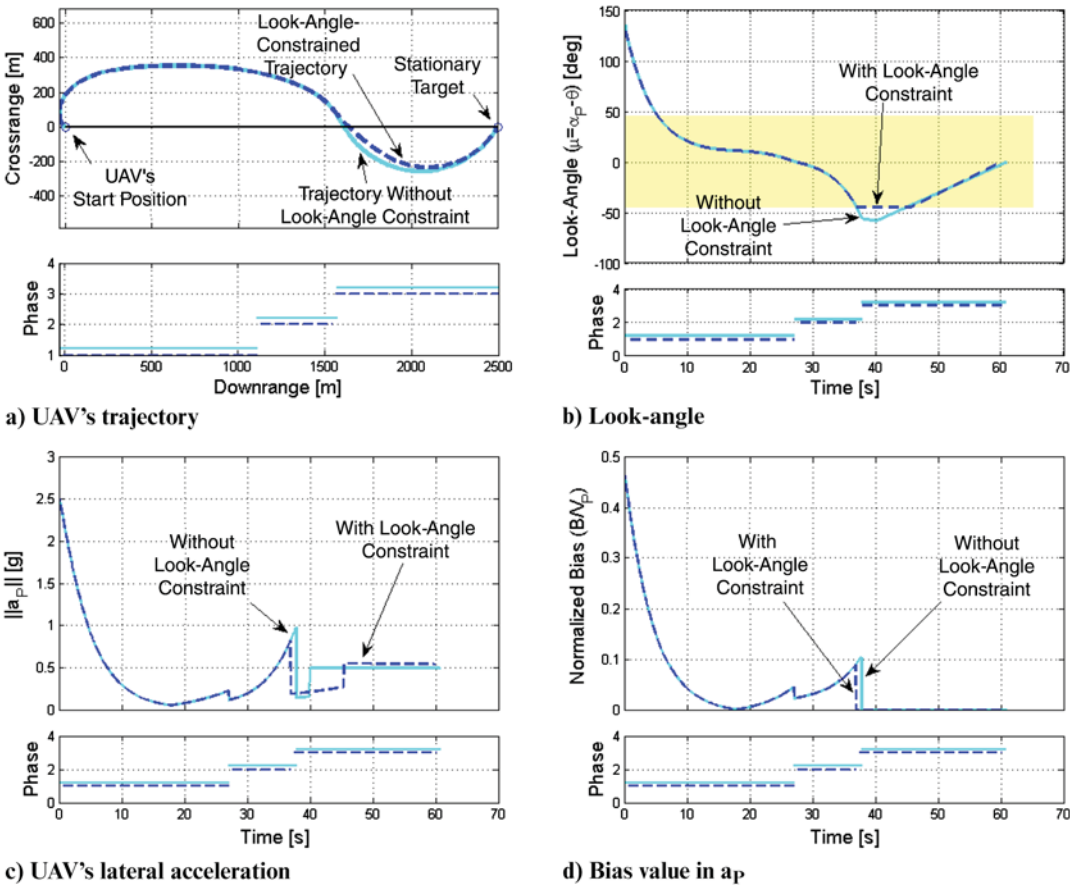

Fig. 7 2-D engagement with $\alpha_{P_f}^d = \pi/3$.

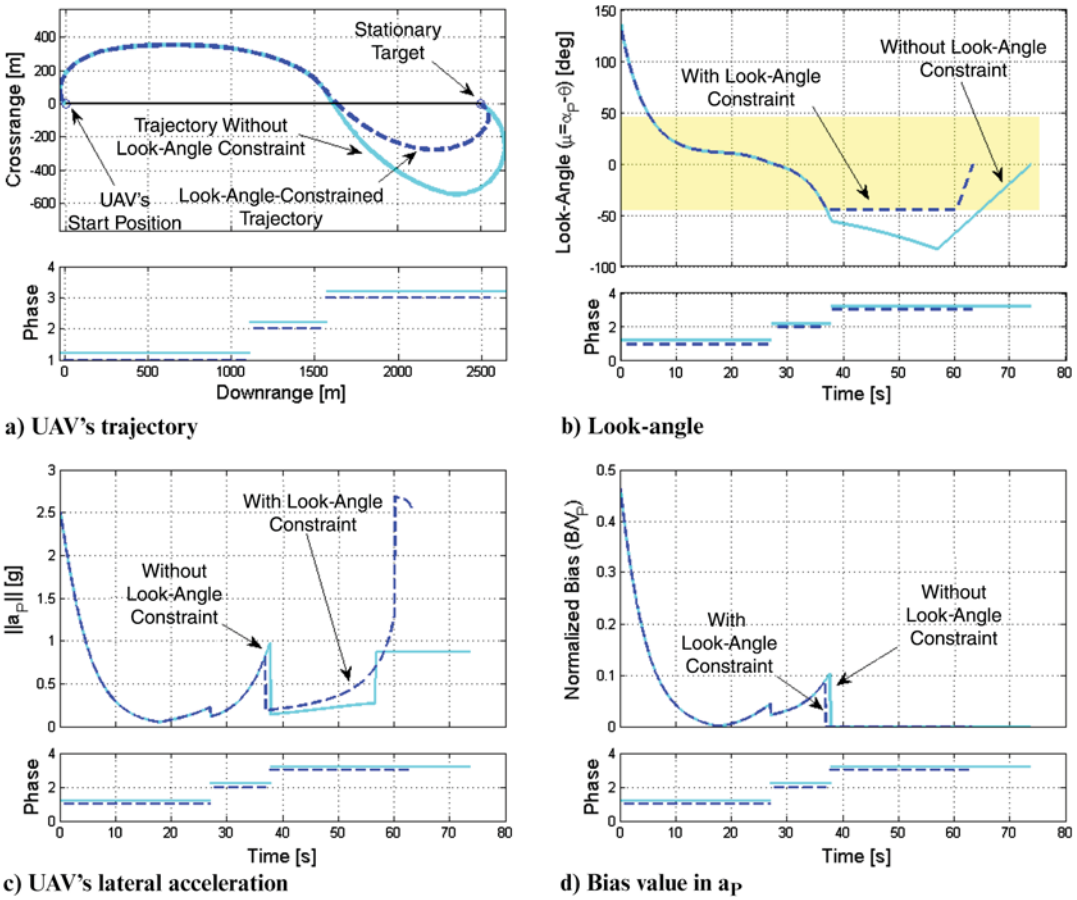

Fig. 8 2-D engagement with $\alpha_{P_f}^d = 5\pi/6$.

Table 1 Summary of the computer simulation results using αCIG and $\mu\alpha$CIG for $\alpha^d_{P_f} = 0, \pi/3, 5\pi/6$

		First phase				Second phase					Third phase
$\alpha^d_{P_f}$, rad	Guidance	N	B	t_2, s	θ_2, rad	N	B	t_3, s	θ_3, rad	μ_3, rad	N
0	αCIG	2	$V_P\|\alpha_P\|/5$	27.05	−0.22	−2	$V_P\|\alpha_P\|/10$	37.8	−0.072	−0.977	14.56
0	$\mu\alpha$CIG	2	$V_P\|\alpha_P\|/5$	27.05	−0.22	−2	$V_P\|\alpha_P\|/10$	36.9	−0.109	−0.782	8.2
$\pi/3$	αCIG	2	$V_P\|\alpha_P\|/5$	27.05	−0.22	−2	$V_P\|\alpha_P\|/10$	37.8	−0.072	−0.977	0.622 (stage 1) 2.001 (stage 2)
$\pi/3$	$\mu\alpha$CIG	2	$V_P\|\alpha_P\|/5$	27.05	−0.22	−2	$V_P\|\alpha_P\|/10$	36.9	−0.109	−0.782	1 (stage 1) 2.0031 (stage 2)
$5\pi/6$	αCIG	2	$V_P\|\alpha_P\|/5$	27.05	−0.22	−2	$V_P\|\alpha_P\|/10$	37.8	−0.072	−0.977	0.622 (stage 1) 2.003 (stage 2)
$5\pi/6$	$\mu\alpha$CIG	2	$V_P\|\alpha_P\|/5$	27.05	−0.22	−2	$V_P\|\alpha_P\|/10$	36.9	−0.109	−0.782	1 (stage 1) 2.0152 (stage 2)

$$\alpha^d_{P_f} \in (\theta_3, \pi + \theta_3] = (-0.109, 3.033] \text{ rad}$$

and at the end of the second phase:

$$\mu = \mu_3 = -0.782 \text{ rad} \in (-\mu_s, 0]$$

Without the look-angle constraint, engagement remains the same until the end of the second phase for all desired α_{P_f} values. However, they deviate from one another at the final phase, depending on $\alpha^d_{P_f}$. In the final phase, PPN guidance is used with $N = 14.56$ to achieve $\alpha^d_{P_f} = 0 \in [\theta_0, 2\theta_3 - \alpha_{P_3}] = [0, 0.905]$ rad. On the other hand, because $\alpha^d_{P_f} = \pi/3, 5\pi/6 \in (2\theta_3 - \alpha_{P_3}, \pi + \theta_0) = (0.905, \pi)$ rad, 2pPPN guidance is used in the final phase with $N = (2/\pi)|\alpha_{P_3} - \theta_3| = 0.622$ as long as $(\alpha^d_{P_f} - \alpha_P)/(\alpha^d_{P_f} - \theta) < 2$; and $N = 2.001$ and $N = 2.003$ otherwise for $\alpha^d_{P_f} = \pi/3$ and $\alpha^d_{P_f} = 5\pi/6$, respectively (see Theorem 1 and Observation 1). These αCIG-guided engagements justify Theorem 3.

Under the look-angle-constrained scenario, the engagements remain the same until the end of the second phase for all desired α_{P_f} values, and they deviate from one another at the final phase depending on $\alpha^d_{P_f}$. The PPN is used in the final phase with $N = 8.2$ to achieve $\alpha^d_{P_f} = 0 \in [\theta_0, 2\theta_3 - \alpha_{P_3}] = [0, 0.673]$ rad. On the other hand, because $\alpha^d_{P_f} = \pi/3, 5\pi/6 \in (2\theta_3 - \alpha_{P_3}, \pi + \theta_0) = (0.673, \pi)$ rad, the look-angle-constrained 2pPPN is used in the final phase with $N = 1$ for $\theta \in [\theta_3, \alpha^d_{P_f} + \mu_3/(N_s - 1))$; and $N = N_s = 2.0031$ and $N = N_s = 2.0152$ otherwise for $\alpha^d_{P_f} = \pi/3$ and $\alpha^d_{P_f} = 5\pi/6$, respectively (see Theorem 4 and Observation 6). These $\mu\alpha$CIG-guided engagements justify Theorem 6. Table 1 summarizes these results on 2-D engagements.

In all simulations, the error in achieving $\alpha^d_{P_f}$ was on the order of 10^{-3} or less. From Figs. 6c, 7c and 8c, it is seen that the UAV's lateral acceleration is usually less than its maximum capability; that is $\|\boldsymbol{a}_P < \|\boldsymbol{a}_{P_{\max}}\|$. Overall, these simulated 2-D engagements justify the results in Theorems 2 and 5 and the composite three-phase guidance schemes, αCIG and $\mu\alpha$CIG, presented in Secs. II.D and III.C, respectively.

As seen from Figs. 6c, 7c, and 8c, the required lateral acceleration of the UAV has discontinuities that arise at the instances of switching the phases. In practice, this command acceleration will then be passed on to the controller. Because the duration of the phases is very large compared to standard autopilot time constants, these discontinuities would be smoothened, and hence have no adverse effect on the overall performance, as can be seen in realistic flight-ready SITL simulation discussed in the next section. Note that the focus of this paper has remained on showing how a bias-based modification of the most widely used PN guidance law can effectively be leveraged to achieve an all-aspect approach angle control at a stationary point. To this end, the existence of such bias profiles has been analyzed so that they satisfy the aforementioned purpose without and with the look-angle constraint. Figure 9 demonstrates the nature of the variation of approach angle-constrained UAV trajectories with the variation of the constant bias profiles applied in αCIG and $\mu\alpha$CIG guidance schemes. It could specifically be noted from Fig. 9 that, in both the cases, with an increase in bias value, the duration of the first two phases (at the end of which the bias is withdrawn) decreases almost exponentially. The advantage of using a higher bias value is that the requirement of a sharp turn in the final phase reduces so that the UAV does not need to pull a high maneuver in the final phase, whereas for very low bias profiles (see trajectories for $B = 0.02V_P$), the trajectories undergo an undesired severe turn, requiring very high lateral acceleration at the final phase. On the other hand, the use of very high bias profiles (see trajectories for $B = 0.3V_P$ and $0.5V_P$) results in a high maneuver during the initial phase. Thus, use of a high bias value would be limited by the maximum maneuverability of the UAV. These indicate that a bias profile could be selected from the feasible set considering a tradeoff between high and low values. However, the criteria of selection of the bias profile from the feasible set for any specific purpose are dependent on several different factors, which constitute another research problem by itself (for example, paper [33] proposes a bias-shaping method based on [30]), and therefore have been kept out of the scope of this paper.

B. 3-D Engagements Using $\mu\alpha$CIG3D

Simulation results for four 3-D engagements are presented in Fig. 10 for the following initial engagement parameters: unit vector along UAV's heading of $\boldsymbol{e}_{P_0} = [-1 \quad 1 \quad 1]/\sqrt{3}$, range of $R_0 = 2500\sqrt{3}$ m, and unit vector along LOS vector $\boldsymbol{e}_{r_0} = [1 \quad 1 \quad 1]/\sqrt{3}$. The unit vector along the initial angular rotation vector of the LOS was

$$\begin{aligned}\boldsymbol{e}_{\Omega_{p1_0}} &= \boldsymbol{\Omega}_{p1_0}/\omega_{p1_0} = \boldsymbol{e}_{r_{p1_0}} \times (-\boldsymbol{v}_{P_0})/\|\boldsymbol{e}_{r_{p1_0}} \times (-\boldsymbol{v}_{P_0})\| \\ &= [0; \quad 1; \quad -1]/\sqrt{2}\end{aligned}$$

Therefore, $\boldsymbol{e}_{t_{p1_0}} = [0.817; \quad -0.408; \quad -0.408]$ and, in the EP_0 plane, $\alpha_{P_{p1_0}} = -1.231$ rad and $\theta_{p1_0} = 0$. The four desired final heading vectors along $\boldsymbol{e}^d_{P_f} = [-1 \quad 1 \quad 1]/\sqrt{3}$ (Case 1), $\boldsymbol{e}^d_{P_f} = [1 \quad -1 \quad 1]/\sqrt{3}$ (Case 2), $\boldsymbol{e}^d_{P_f} = [1 \quad 1 \quad -1]/\sqrt{3}$ (Case 3), and $\boldsymbol{e}^d_{P_f} = [-1 \quad -1 \quad 1]/\sqrt{3}$ (Case 4) were considered. The UAV's trajectories, and their projections on the (XY), (XZ), and (YZ) planes, along with UAV's look angle, magnitude of lateral acceleration, and normalized bias profiles, are plotted in Figs. 10a–10g, respectively.

In Case 1 ($\boldsymbol{e}^d_{P_f} = [-1 \quad 1 \quad 1]/\sqrt{3}$), because $\boldsymbol{e}^d_{P_f} = \boldsymbol{e}_{P_0}$, the engagement is actually planar with the EP_0 plane spanned by $\boldsymbol{e}_{r_0} = [1 \quad 1 \quad 1]/\sqrt{3}$ and $\boldsymbol{e}_{P_0} = [-1 \quad 1 \quad 1]/\sqrt{3}$. Therefore, $\beta = 1$; that is, the VT coincides with the actual stationary target, and the engagement ends with the first planar phase in EP_0. Following Step 1 of the first planar phase of $\mu\alpha$CIG3D in Sec. IV.C, $\alpha_{P_0} = \alpha^d_{P_f} = -1.231$ rad $\in (-\pi, 0]$ in EP_0. Therefore, following Step 5 of the first planar phase, a three-phase composite guidance strategy is applied to achieve $\boldsymbol{e}^d_{P_f}$. The BPPN with $N = 2$ and $B = V_P|\alpha_P|/5$ is applied in the first phase, which ends at a time of $t_2 = 33.3$ s, and the second phase begins with $N = -2$ and $B = V_P|\alpha_P|/10$. The second phase ends at a time of $t_3 = 50.75$ s, when in EP_0, $\theta_3 = -0.008$ rad, $\alpha_3 = 0.773$ rad, and thus $\mu_3 = 0.781$ rad remains within the FOV limit of $\mu_s = \pi/4$, whereas $\alpha^d_{P_{p1_f}} = -1.231$ rad $\in [-\pi + \theta_3, \theta_3) = [-3.15, -0.008)$ rad. The look-angle-constrained 2pPPN is used in the third phase with $N = 1$ and 2.002 in the initial and final stages of

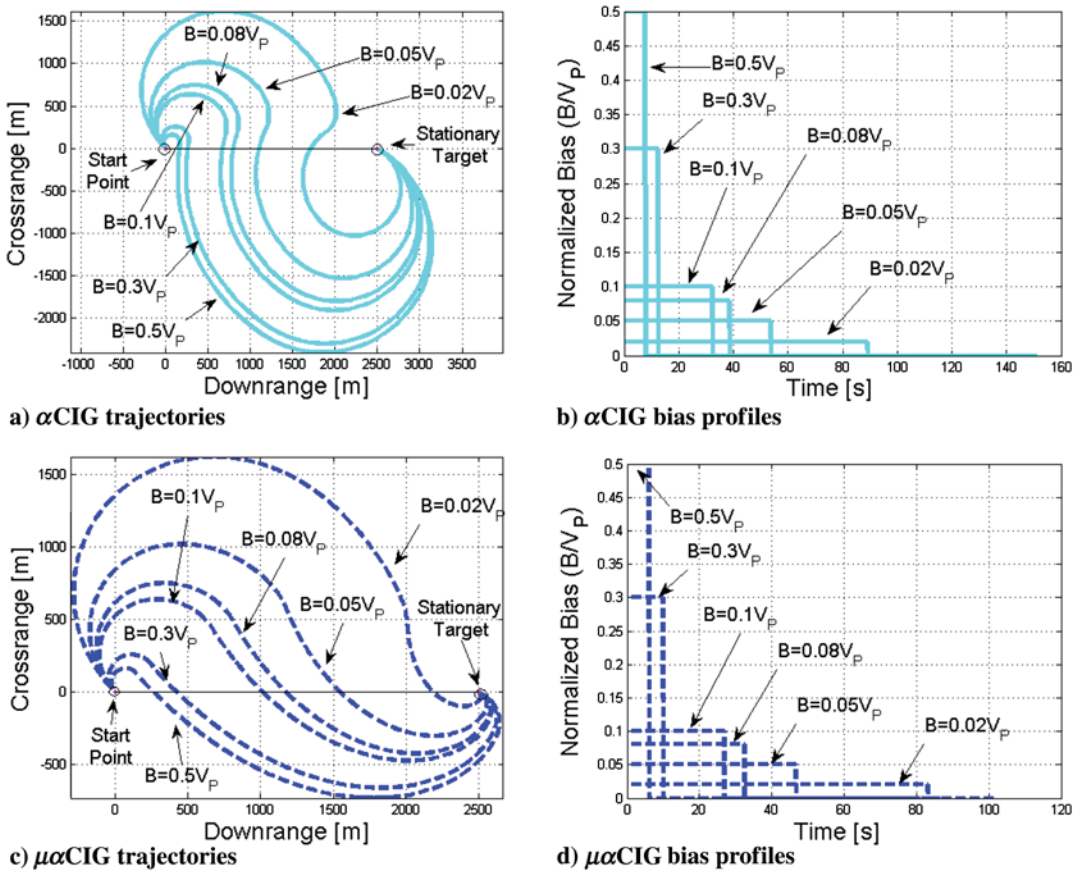

Fig. 9 αCIG and $\mu\alpha$CIG with varied constant bias profiles.

the third phase. The norm of error in the achieved approach vector is 0.001.

On the other hand, in Cases 2–4, $\boldsymbol{e}_{r_0}$, $\boldsymbol{e}_{P_0}$, and $\boldsymbol{e}^d_{P_f}$ are not coplanar; hence, the engagements are nonplanar. Therefore, the engagements consist of two planar phases as described in Secs. IV.C and IV.D. The VT position is fixed with $\beta = 0.5$; that is, $\boldsymbol{r}_{\mathrm{VT}} = 1250[1 \quad 1 \quad 1]$ m. At the end of the first planar phase in the EP_0 plane, spanned by $\boldsymbol{e}_{r_0} = [1 \quad 1 \quad 1]/\sqrt{3}$ and $\boldsymbol{e}_{P_0} = [-1 \quad 1 \quad 1]/\sqrt{3}$, the UAV's desired position and heading are $\boldsymbol{r}_{\mathrm{VT}}$ and along $\boldsymbol{e}_{r_0}$, respectively; that is, $\alpha^d_{P_{p1_f}} = 0$. Following Step 5 of the first planar phase of $\mu\alpha$CIG3D in Sec. IV.C, $N = 2, -2$, and 10.645 and $B = |\alpha_P|/5, |\alpha_P|/5, 0$ are used in the first through the third phases, respectively. Because the initial and desired final conditions for the engagement in EP_0 are the same for these cases, the trajectories, look-angle, lateral acceleration, and bias profiles of the UAV in this planar phase are identical as well. The first phase ends at a time of $t_2 = 23.35$ s when the LOS angle with respect to the VT of $\theta_{p1}(t_2) = \theta_2 = 0.171$ rad, at which the LOS (with respect to VT) turn rate reverses its sign. The second phase ends at time of $t_3 = 29.65$ s with $\theta_3 = 0.081$ rad and $\alpha_{P_3} = 0.859$ rad; thus, the look angle of $\mu_3 = 0.778$ rad remains within the FOV limit of $\mu_s = \pi/4$, whereas $\alpha^d_{P_{p1_f}} = 0 \in [-\pi + \theta_3, \theta_3) = [-3.061, 0.081)$ rad. The third phase ends, and the second planar phase begins at a time of $t_4 = 45.65$ s when the UAV gets very close (1.34 m) to the VT and its heading is aligned with $\boldsymbol{e}_{r_0}$.

In the second planar phase for Cases 2–4, the engagements occur in the different EP_f planes, which are formed by $\boldsymbol{e}_{r_{P2_0}} = \boldsymbol{e}_{r_0}$ and the corresponding different $\boldsymbol{e}^d_{P_f}$ vectors. Hence, they are all different. The engagement in EP_f starts at $t_4 = 45.65$ s with $\alpha_{P_{p2_0}} = \theta_{p2_0} = 0$. Following Step 1 of the second planar phase of $\mu\alpha$CIG3D in Sec. IV.D, $\boldsymbol{e}_{\boldsymbol{\Omega}_{p2_0}}$ and $\boldsymbol{e}_{\boldsymbol{t}_{p2_0}}$ are obtained for Case 2 ($\boldsymbol{e}^d_{P_f} = [1 \quad -1 \quad 1]/\sqrt{3}$), Case 3 ($\boldsymbol{e}^d_{P_f} = [1 \quad 1 \quad -1]/\sqrt{3}$), and Case 4 ($\boldsymbol{e}^d_{P_f} = [-1 \quad -1 \quad 1]/\sqrt{3}$); and values of $\alpha^d_{P_f}$ are obtained as 1.231, 1.231, and 1.911 rad, respectively. Following Step 2 of this planar phase, an adjustment bias guidance with $b_{\mathrm{adj}} = 0.1V_P$ is applied in the fourth phase until $\theta_{p2} = \theta_5 = 0.0664$, 0.0664, 0.0657 rad for Cases 2–4, respectively, such that $\alpha^d_{P_f} \in (\theta_5, \pi]$ in respective cases. The look angles $\mu_5 = -0.781$ rad, $\mu_5 = -0.781$ rad, and $\mu_5 = -0.776$ rad, respectively, remain within the FOV constraint $\mu_s = \pi/4$. At $t_5 = 52.8$ s for Cases 2 and 3, and $t_5 = 52.75$ s for Case 4, the fifth phase (final phase) begins. In the final phase, the look-angle-constrained 2pPPN guidance scheme is applied with $N = 1$ during the initial stage and $N = 2.002$ during the final stage for all cases. Table 2 summarizes these results on 3-D engagements.

As in the case of 2-D engagements, the norm of errors in achieved $\boldsymbol{e}^d_{P_f}$ is found to be 0.002, and $\|\boldsymbol{a}_P\| < \|\boldsymbol{a}_{P_{\max}}\|$.

VI. SITL Simulation Results

The guidance algorithms presented in this paper are currently tuned to be implemented on a fixed-wing UAV (the NPS Zephyr-II) featuring a wingspan of around 1.45 m and a nominal endurance of about 50 min (shown in Fig. 11a) [47]. The onboard avionics suite includes the Pixhawk ArduPlane autopilot, which is capable of executing waypoint (WP) navigation. To handle higher-level planning and coordination tasks, the onboard computer (an ODroid U3) runs robot operating software nodes that implement autonomous behaviors in a multi-UAV setup. In case of necessary interaction with an individual UAV, a redundant communication path following the MAVLink communication protocol is used via the 3D Robotics (3DR) serial modem radio [48]. To facilitate live-fly UAV field experiments, a SITL simulation setup that allows testing with a flight-ready software environment is employed as shown in Fig. 11b. This setup includes the flight dynamics simulator JSBSim, which models aerodynamics, propulsion, and six-degree-of-freedom equations of flight motion [49]; ArduPlane desktop executable autopilot software, and a 3DR MAVProxy ground control station (GCS) interface [50].

An example of a SITL simulation in 2-D engagement with the αCIG strategy, discussed in Sec. II.D, is presented in Figs. 12 and 13. Specifically, the bird's-eye view of the UAV's trajectory is shown in

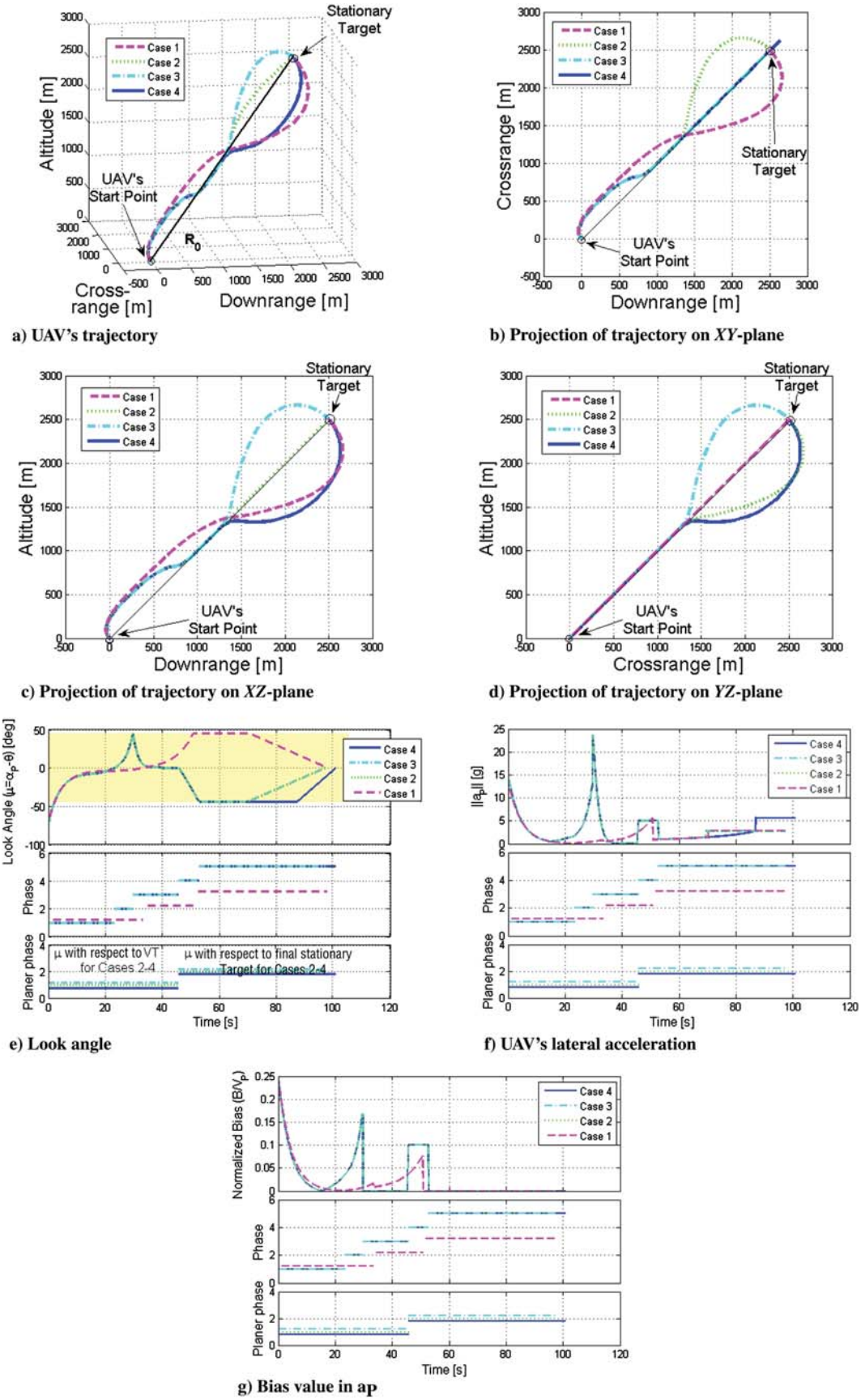

Fig. 10 3-D engagements for four desired approach vectors.

Fig. 12a. The initial location of the UAV is at (143.1,147.1) m, and the stationary target is located at (599.5,0) m at the same altitude. Thus, $\theta_0 = -0.31$ rad (-17.9 deg), $\alpha_{P_0} = 0.2$ rad (11.4 deg), and $\alpha^d_{P_f} = 0.7$ rad (39.6 deg). Because $\alpha_{P_0} > \theta_0$ and $\alpha^d_{P_f} \in [\theta_0, \pi + \theta_0)$, the three-phase composite guidance scheme mentioned in Step 3 of αCIG would be a suitable choice for this engagement. The BPPN guidance with $N = 2$ and $B = 0.5V_P$ is applied in the first phase, which ends with $\theta_2 = -0.34$ rad (-19.3 deg). The BPPN is

Table 2 Summary of the computer simulation results using $\mu\alpha$CIG3D for four cases

	Engagement in EP_0										Engagement in EP_f			
	First phase			Second phase				Third phase			Fourth phase			Fifth phase
$\boldsymbol{e}^d_{P_f}$, m	N	B	t_2, s	N	B	t_3, s	μ_3, rad	N	t_4, s	μ_4, rad	B	t_5, s	μ_5, rad	N
$[-1 \quad 1 \quad 1]/\sqrt{3}$ (planar)	2	$V_P\lvert\alpha_P\rvert/5$	33.3	−2	$V_P\lvert\alpha_P\rvert/10$	50.75	0.781	1 (stage 1) 2.002 (stage 2)	— —	— —	— —	— —	— —	— —
$[1 \quad -1 \quad 1]/\sqrt{3}$	2	$V_P\lvert\alpha_P\rvert/5$	23.35	−2	$V_P\lvert\alpha_P\rvert/5$	29.65	0.778 (with respect to VT)	10.6453	45.65	0	$0.1V_P$	52.8	−0.781	1 (stage 1) 2.002 (stage 2)
$[1 \quad 1 \quad -1]/\sqrt{3}$	2	$V_P\lvert\alpha_P\rvert/5$	23.35	−2	$V_P\lvert\alpha_P\rvert/5$	29.65	0.778 (with respect to VT)	10.6453	45.65	0	$0.1V_P$	52.8	−0.781	1 (stage 1) 2.002 (stage 2)
$[-1 \quad -1 \quad 1]/\sqrt{3}$	2	$V_P\lvert\alpha_P\rvert/5$	23.35	−2	$V_P\lvert\alpha_P\rvert/5$	29.65	0.778 (with respect to VT)	10.6453	45.65	0	$0.1V_P$	52.75	−0.776	1 (stage 1) 2.002 (stage 2)

continued into the second phase with $N = -2$ and $B = 0.25V_P$, and it ends with $\theta_3 = -0.32$ rad (−18.1 deg), followed by the 2pPPN guidance in the final phase. To implement the UAV's guidance command a_P in a SITL simulation, the WPs $(x_{L_{1_P}}, y_{L_{1_P}})$ are generated as

$$x_{L_{1_P}} = x_P + L_1\cos(\alpha_P + \eta);$$
$$y_{L_{1_P}} = y_P + L_1\cos(\alpha_P + \eta);$$
$$\eta = \sin^{-1}(k_1 a_P L_1/2V_P^2) \tag{26}$$

where (x_P, y_P) are the instantaneous coordinates of the UAV; L_1 is the projected range to the next WP; η is the angle to the next WP; and k_1 is a tuning parameter, which could be chosen for satisfactory performance. In the demonstrated example, the two variable parameters L_1 and k_1 are chosen as $L_1 = 150$ m and $k_1 = 1$. The frequency of the UAV's WP command generation is 10 Hz. The SITL simulation ends when the UAV reaches the target within a 25 m distance (a safety separation fence).

The UAV's final approach angle is $\alpha_{P_f} = 0.59$ rad (33.8 deg), which is approximately 0.1 l rad (6.2 deg) apart from $\alpha^d_{P_f}$. It should be noted that the algorithm produces a feasible solution, even in the real-world

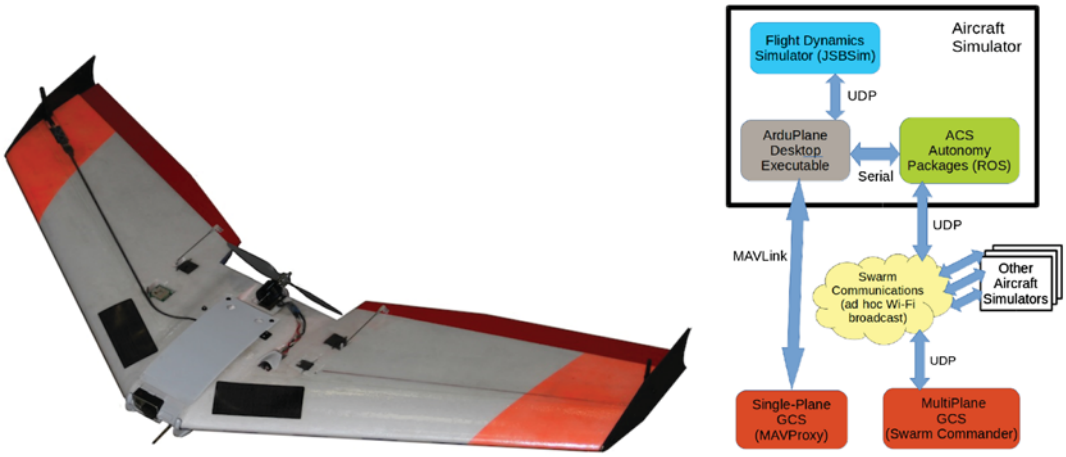

a) Testbed NPS zephyr-II UAV b) SITL simulator block diagram

Fig. 11 Testbed UAV [47] and SITL simulation platform [48] (ROS, robot operating system; UDP, user datagram protocol).

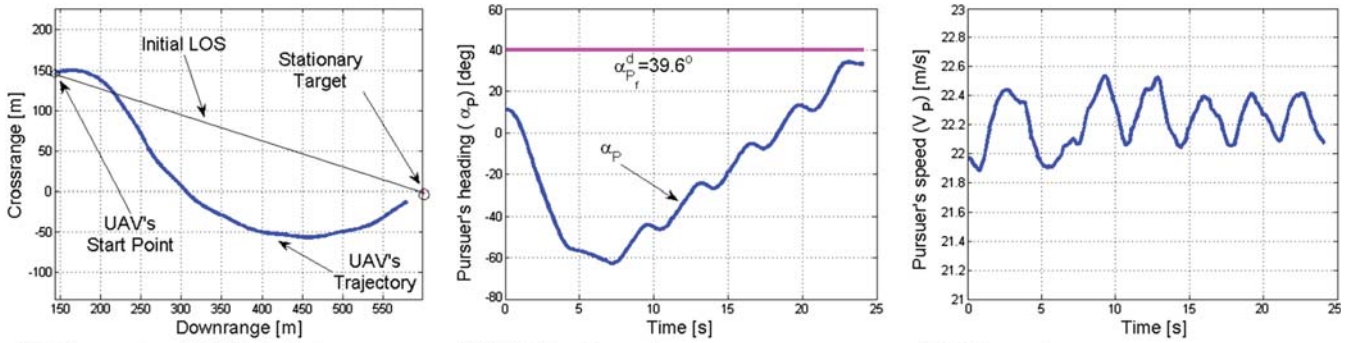

a) Bird's eye-view of UAV's trajectory b) UAV's heading angle c) UAV's speed

Fig. 12 SITL simulation of 2-D engagement.

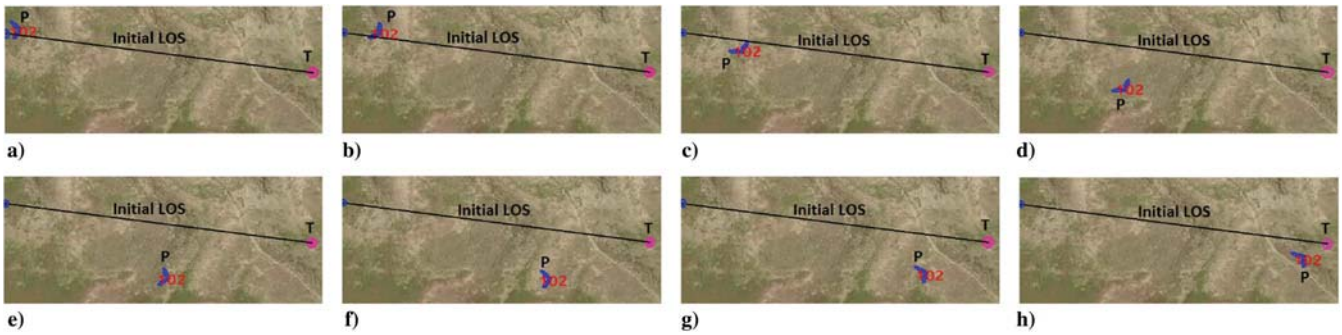

Fig. 13 Snapshots of an illustrative run of the SITL simulation: a–b) first and second phases, and c–h) third phase.

situation when the UAV speed is changing due to the varying drag while the airspeed controller tries to keep it constant (see Fig. 12c).

A sequence of snapshots of the SITL simulation in the geographic environment, where the actual flight tests are conducted, is shown in Fig. 13.

VII. Conclusions

This paper presented a complete set of the pure proportional navigation-based integrated guidance strategies for approaching a stationary point from any given direction. Specifically, the three-phase composite guidance law is derived to complement the standard and two-stage pure proportional navigation guidance laws. The derivations also include modifications to the algorithm to account for a field-of-view limitation imposed by an onboard sensor. The two-dimensional case is extended to a two-plane-segregated two-planar-phase guidance scheme to control the approach vector in the three-dimensional case. Computer and software-in-the-loop simulations for a small unmanned aerial vehicle proved the developed integrated guidance scheme to be a viable and ready-to-implement option for a trajectory-shape-varying approach to a stationary target.

Acknowledgments

The authors would like to thank the Consortium for Robotics and Unmanned Systems Education and Research at the Naval Postgraduate School for funding this research.

References

[1] Rysdyk, R., "Unmanned Aerial Vehicle Path Following for Target Observation in Wind," *Journal of Guidance, Control, and Dynamics*, Vol. 29, No. 5, Sept.–Oct. 2006, pp. 1092–1100. doi:10.2514/1.19101

[2] Park, S., Deyst, J., and How, J. P., "Performance and Lyapunov Stability of a Nonlinear Path-Following Guidance Method," *Journal of Guidance, Control, and Dynamics*, Vol. 30, No. 6, Nov.–Dec. 2007, pp. 1718–1728. doi:10.2514/1.28957

[3] Yamasaki, T., Sakaida, H., and Enomoto, K., "Robust Trajectory-Tracking Method for UAV Guidance Using Proportional Navigation," *Proceedings of the International Conference on Control, Automation, and Systems*, IEEE Publ., Piscataway, NJ, Oct. 2007, pp. 1404–1409. doi:10.1109/ICCAS.2007.4406558

[4] Smith, A. L., "Proportional Navigation with Adaptive Terminal Guidance for Aircraft Rendezvous," *Journal of Guidance, Control, and Dynamics*, Vol. 31, No. 6, Nov.–Dec. 2008, pp. 1832–1836. doi:10.2514/1.33535

[5] Han, S. C., Bang, H., and Yoo, C. S., "Proportional Navigation-Based Collision Avoidance for UAVs," *International Journal of Control, Automation, and Systems*, Vol. 7, No. 4, 2009, pp. 553–565. doi:10.1007/s12555-009-0407-1

[6] Clark, M., and Prazenica, R. J., "Vision-Based Proportional Navigation for UAS Collision Avoidance," *AIAA Guidance, Navigation, and Control Conference*, AIAA Paper 2016-1986, Jan. 2016. doi:10.2514/6.2016-1986

[7] Clark, M., and Prazenica, R. J., "Proportional Navigation Based Guidance Laws for UAV Obstacle Avoidance in Complex Urban Environments," *AIAA Guidance, Navigation, and Control Conference*, AIAA Paper 2017-0672, Jan. 2017. doi:10.2514/6.2017-0672

[8] Kim, M., and Grider, K. V., "Terminal Guidance for Impact Attitude Angle Constrained Flight Trajectories," *IEEE Transactions on Aerospace and Electronic Systems*, Vol. AES-9, No. 6, Nov. 1973, pp. 852–859. doi:10.1109/TAES.1973.309659

[9] Idan, M., Golan, O., and Guelman, M., "Optimal Planar Interception with Terminal Constraints," *Journal of Guidance, Control, and Dynamics*, Vol. 18, No. 6, Nov.–Dec. 1995, pp. 1273–1279. doi:10.2514/3.21541

[10] Ryoo, C. K., Cho, H., and Tahk, M. J., "Optimal Guidance Laws with Terminal Impact Angle Constraint," *Journal of Guidance, Control, and Dynamics*, Vol. 28, No. 4, July–Aug. 2005, pp. 724–732. doi:10.2514/1.8392

[11] Ryoo, C. K., Cho, H., and Tahk, M. J., "Time-to-Go Weighted Optimal Guidance with Impact Angle Constraints," *IEEE Transactions on Control Systems Technology*, Vol. 14, No. 3, May 2006, pp. 483–492. doi:10.1109/TCST.2006.872525

[12] Ohlmeyer, E. J., and Phillips, C. A., "Generalized Vector Explicit Guidance," *Journal of Guidance, Control, and Dynamics*, Vol. 29, No. 2, March–April 2006, pp. 261–268. doi:10.2514/1.14956

[13] Harrison, G. A., "Hybrid Guidance Law for Approach Angle and Time-of-Arrival Control," *Journal of Guidance, Control, and Dynamics*, Vol. 35, No. 4, July–Aug. 2012, pp. 1104–1114. doi:10.2514/1.56131

[14] Shaferman, V., and Shima, T., "Linear Quadratic Guidance Laws for Imposing a Terminal Intercept Angle," *Journal of Guidance, Control, and Dynamics*, Vol. 31, No. 5, Sept.–Oct. 2008, pp. 1400–1412. doi:10.2514/1.32836

[15] Rusnak, I., Weiss, H., Eliav, R., and Shima, T., "Missile Guidance with Constrained Intercept Body Angle," *IEEE Transactions on Aerospace and Electronic Systems*, Vol. 50, No. 2, March 2014, pp. 1445–1453. doi:10.1109/TAES.2014.120100

[16] Park, B. G., Kim, T. H., and Tahk, M. J., "Optimal Impact Angle Control Guidance Law Considering the Seeker's Field-of-View Limits," *Journal of Aerospace Engineering*, Vol. 227, No. 8, Aug. 2013, pp. 1347–1364. doi:10.1177/0954410012452367

[17] Cho, H., Ryoo, C. K., Tsourdos, A., and White, B., "Optimal Impact Angle Control Guidance Law Based on Linearization About Collision Triangle," *Journal of Guidance, Control, and Dynamics*, Vol. 37, No. 3, May–June 2014, pp. 958–964. doi:10.2514/1.62910

[18] Ratnoo, A., and Ghose, D., "State-Dependent Riccati-Equation-Based Guidance Law for Impact-Angle-Constrained Trajectories," *Journal of Guidance, Control, and Dynamics*, Vol. 32, No. 1, Jan.–Feb. 2009, pp. 320–326. doi:10.2514/1.37876

[19] Bardhan, R., and Ghose, D., "Nonlinear Differential Games-Based Impact-Angle-Constrained Guidance Law," *Journal of Guidance, Control, and Dynamics*, Vol. 38, No. 3, March 2015, pp. 384–402. doi:10.2514/1.G000940

[20] Shima, T., "Intercept-Angle Guidance," *Journal of Guidance, Control, and Dynamics*, Vol. 34, No. 2, March–April 2011, pp. 484–492. doi:10.2514/1.51026

[21] Kumar, S. R., Rao, S., and Ghose, D., "Sliding-Mode Guidance and Control for All-Aspect Interceptors with Terminal Angle Constraints," *Journal of Guidance, Control, and Dynamics*, Vol. 35, No. 4, July–Aug. 2012, pp. 1230–1246. doi:10.2514/1.55242

[22] Harl, N., and Balakrishnan, S. N., "Impact Time and Angle Guidance with Sliding Mode Control," *IEEE Transactions on Control Systems*

Technology, Vol. 20, No. 6, Nov. 2012, pp. 1436–1449.
doi:10.1109/TCST.2011.2169795

[23] Kumar, S. R., Rao, S., and Ghose, D., "Nonsingular Terminal Sliding Mode Guidance with Impact Angle Constraints," *Journal of Guidance, Control, and Dynamics*, Vol. 37, No. 4, July–Aug. 2014, pp. 1114–1130.
doi:10.2514/1.62737

[24] Kumar, S. R., and Ghose, D., "Three-Dimensional Impact Angle Guidance with Coupled Engagement Dynamics," *Journal of Aerospace Engineering*, Vol. 231, No. 4, April 2017, pp. 621–641.
doi:10.1177/0954410016641442

[25] Chabra, S., and Talole, S. E., "Fuzzy Logic-Based Terminal Guidance with Impact Angle Control," *Defence Science Journal*, Vol. 57, No. 4, July 2007, pp. 351–360.

[26] Kim, B. S., Lee, J. G., and Han, H. S., "Biased PNG Law for Impact with Angular Constraint," *IEEE Transactions on Aerospace and Electronic Systems*, Vol. 34, No. 1, Jan. 1998, pp. 277–288.
doi:10.1109/7.640285

[27] Lu, P., Doman, D. B., and Schierman, J. D., "Adaptive Terminal Guidance for Hypervelocity Impact in Specified Direction," *Journal of Guidance, Control, and Dynamics*, Vol. 29, No. 2, March–April 2006, pp. 269–278.
doi:10.2514/1.14367

[28] Ratnoo, A., and Ghose, D., "Impact Angle Constrained Interception of Stationary Targets," *Journal of Guidance, Control, and Dynamics*, Vol. 31, No. 6, Nov.–Dec. 2008, pp. 1817–1822.
doi:10.2514/1.37864

[29] Ratnoo, A., and Ghose, D., "Impact Angle Constrained Guidance Against Nonstationary Nonmaneuvering Targets," *Journal of Guidance, Control, and Dynamics*, Vol. 33, No. 1, Jan.–Feb. 2010, pp. 269–275.
doi:10.2514/1.45026

[30] Erer, K. S., and Merttopcuoglu, O., "Indirect Impact-Angle-Control Against Stationary Targets Using Biased Pure Proportional Navigation," *Journal of Guidance, Control, and Dynamics*, Vol. 35, No. 2, March–April 2012, pp. 700–704.
doi:10.2514/1.52105

[31] Ghosh, S., Ghose, D., and Raha, S., "Composite Guidance for Impact Angle Control Against Higher Speed Targets," *Journal of Guidance, Control, and Dynamics*, Vol. 39, No. 1, Jan. 2016, pp. 98–117.
doi:10.2514/1.G001232

[32] Ghosh, S., Davis, D. T., and Chung, T. H., "A Guidance Law for Avoiding Specific Approach Angles Against Maneuvering Targets," *Proceedings of the IEEE Conference on Decision and Control*, IEEE, Piscataway, NJ, Dec. 2016, pp. 4142–4147.
doi:10.1109/CDC.2016.7798897

[33] Kim, T. H., Park, B. G., and Tahk, M. J., "Bias-Shaping Method for Biased Proportional Navigation with Terminal-Angle Constraint," *Journal of Guidance, Control, and Dynamics*, Vol. 36, No. 6, Nov.–Dec. 2013, pp. 1810–1816.
doi:10.2514/1.59252

[34] Tekin, R., and Erer, K. S., "Switched-Gain Guidance for Impact Angle Control Under Physical Constraints," *Journal of Guidance, Control, and Dynamics*, Vol. 38, No. 2, Feb. 2015, pp. 205–216.
doi:10.2514/1.G000766

[35] Ratnoo, A., "Analysis of Two-Stage Proportional Navigation with Heading Constraints," *Journal of Guidance, Control, and Dynamics*, Vol. 39, No. 1, Jan. 2016, pp. 156–164.
doi:10.2514/1.G001262

[36] Manchester, I. R., and Savkin, A. V., "Circular-Navigation-Guidance Law for Precision Missile/Target Engagements," *Journal of Guidance, Control, and Dynamics*, Vol. 29, No. 2, March–April 2006, pp. 314–320.
doi:10.2514/1.13275

[37] Yoon, M. G., "Relative Circular Navigation Guidance for the Impact Angle Control Problem," *IEEE Transactions on Aerospace and Electronic Systems*, Vol. 44, No. 4, Oct. 2008, pp. 1449–1463.
doi:10.1109/TAES.2008.4667721

[38] Tsalik, R., and Shima, T., "Inscribed Angle Guidance," *Journal of Guidance, Control, and Dynamics*, Vol. 38, No. 1, Jan. 2015, pp. 30–40.
doi:10.2514/1.G000468

[39] Zbikowski, R., Shanmugavel, M., Tsourdos, A., and White, B. A., "Path Planning of Multiple UAVs Using Dubins Sets," *AIAA Guidance, Navigation, and Control Conference*, AIAA Paper 2005-5827, Aug. 2005.
doi:10.2514/6.2005-5827

[40] Shanmugavel, M., Tsourdos, A., Zbikowski, R., and White, B. A., "3D Dubins Sets Based Coordinated Path Planning for Swarm of UAVs," *AIAA Guidance, Navigation, and Control Conference*, AIAA Paper 2006-6211, Aug. 2006.
doi:10.2514/6.2006-6211

[41] Hota, S., and Ghose, D., "Optimal Trajectory Planning for Unmanned Aerial Vehicles in Three-Dimensional Space," *Journal of Aircraft*, Vol. 51, No. 2, March–April 2014, pp. 681–688.
doi:10.2514/1.C032245

[42] Zarchan, P., *Tactical and Strategic Missile Guidance*, Vol. 239, Progress in Astronautics and Aeronautics, 6th ed., AIAA, Reston, VA, 2012, pp. 14–0.

[43] Shneydor, N. A., *Missile Guidance and Pursuit–Kinematics, Dynamics and Control*, Harwood Publishing, Chichester, England, U.K., 1998, pp. 101–105.

[44] Dhananjay, N., and Ghose, D., "Accurate Time-to-Go Estimation for Proportional Navigation Guidance," *Journal of Guidance, Control and Dynamics*, Vol. 37, No. 4, July–Aug. 2014, pp. 1378–1383.
doi:10.2514/1.G000082

[45] Apostol, T. M., *Mathematical Analysis*, Narosa Publishing House, New Delhi, India, 2002, pp. 127–133, 140–160.

[46] Tyan, F., "Unified Approach to Missile Guidance Laws: A 3D Extension," *IEEE Transactions on Aerospace and Electronic Systems*, Vol. 41, No. 4, Oct. 2005, pp. 1178–1199.
doi:10.1109/TAES.2005.1561882

[47] Chung, T. H., Clement, M. R., Day, M. A., Jones, K., Davis, D., and Jones, M., "Live-Fly, Large-Scale Field Experimentation for Large Numbers of Fixed-Wing UAVs," *Proceedings of the IEEE International Conference on Robotics and Automation*, IEEE Publ., Piscataway, NJ, May 2016, pp. 1255–1262.
doi:10.1109/ICRA.2016.7487257

[48] Day, M. A., Clement, M. R., Russo, J. D., Davis, D., and Chung, T. H., "Multi-UAV Software Systems and Simulation Architecture," *Proceedings of the International Conference on Unmanned Aerial Systems*, IEEE Publ., Piscataway, NJ, June 2015, pp. 426–435.
doi:10.1109/ICUAS.2015.7152319

[49] "JSBSim Open Source Flight Dynamics Model in C++," *Sourceforge.net*, Oct. 2016, http://jsbsim.sourceforge.net/JSBSimFlyer.pdf [retrieved 2017].

[50] "SITL Simulator (Software in the Loop)," *Ardupilot.org*, Oct. 2016, http://ardupilot.org/dev/docs/sitl-simulator-software-in-the-loop.html [retrieved 2017].